Paul Josef Krassnig, BSc

Numerical modelling of the temperature dependence of NQR transition frequencies in molecular crystals

MASTER‘S THESIS

Institute of Medical Engineering
Graz University of Technology
Head: Univ.-Prof. Dipl.-Ing. Dr.techn. Rudolf Stollberger

Supervisor: Ao.Univ.-Prof. Dipl.-Ing. Dr.techn. Scharfetter Hermann
Dipl.-Ing. Gösweiner Christian, BSc

Graz, May 2019

Aknowledgements

Special thanks to all my supporters who made this Thesis possible:

Institute of Medical Engineering: Prof. Scharfetter, Prof. Stollberger, Christina, Stefan, Oliver, Walter, Dani, Matthias, Christoph, Andi L., Andi P., Markus, Markus M. and "Mr. NQR" Christian

My beloved family: Mama, Papa und Samy
Tante Biene mit Sultan

& friends: Gabriel and all PuJ members

"Donk'schen"

AFFIDAVIT

I declare that I have authored this thesis independently, that I have not used other than the declared sources/resources, and that I have explicitly indicated all material which has been quoted either literally or by content from the sources used. The text document uploaded to TUGRAZonline is identical to the present master‘s thesis dissertation.

Graz, …… ……..

(Signature)

Abstract

In the course of the FET-Open project “CONQUER”, Bi-aryl compounds proved to be promising in terms of their physical and chemical properties to enable quadrupole relaxation enhancement. Knowledge of Bi-aryl compound’s temperature sensitivity is of great importance to predict the desired frequency crossing of NQR transition frequencies and the Larmor frequency of protons at certain field strength more precisely. The aim of this master’s thesis is to model the temperature dependence of NQR transition frequencies of Triphenylbismuth and Tris(2-methoxyphenyl)bismuthine based on molecular motions, precisely torsional oscillations. The focus is set on numerical modelling to overcome commonly applied assumptions and approximations, which are constant asymmetry parameter of the electric field gradient η and small angle approximation of torsional oscillations, used by analytical models. Their influence on modeled NQR transition frequencies as well as benefits of numerical implementations are displayed and analyzed. Furthermore, a novel numerical fitting approach, involving two NQR transition frequencies at once (increased data set for fitting), is presented. Obtained fitting parameters of Triphenylbismuth, such as torsional frequency and equivalent moment of inertia, of analytical and numerical models are comparable and have plausible orders of magnitude. Generally, Triphenylbismuth shows a greater response to temperature than Tris(2-methoxyphenyl)bismuthine. Interestingly, numerical simulations of different torsional oscillation directions revealed to have an impact on the sign of the temperature coefficient of the lowest transition in case of an axially asymmetric electric field gradient. Finally, important aspects and improvements concerning future modelling processes of the temperature dependence of NQR transition frequencies are proposed.

Keywords: NQRS, Triphenylbismuth, Tris(2-methoxyphenyl)bismuthine, temperature sensitivity, numerical modelling

Zusammenfassung

Im Rahmen des FET-Open-Projekts "CONQUER" stellten sich Bi-aryl-Verbindungen in ihren physikalischen und chemischen Eigenschaften als vielversprechend heraus um Quadrupole-Relaxation-Enhancement zu ermöglichen. Die Kenntnis der Temperatursensitivität von Bi-aryl-Verbindungen ist von großer Bedeutung um das gewünschte Frequency-Crossing von NQR-Übergangsfrequenzen und der Larmorfrequenz von Protonen bei bestimmten Feldstärken genauer vorherzusagen. Ziel dieser Masterarbeit ist es daher, die Temperaturabhängigkeit der NQR-Übergangsfrequenzen von Triphenylbismuth und Tris(2-methoxyphenyl)bismuthine basierend auf molekularen Bewegungen, genauer gesagt ihrer Torsionsschwingungen zu modellieren. Um gängige Annahmen (konstanter Asymmetrieparameter des elektrischen Feldgradienten η) und Approximationen (kleine Winkel der Torsionsschwingungen) analytischer Modelle zu überwinden, liegt der Schwerpunkt auf numerischer Modellierung. Einfluss dieser Annahmen und Approximationen auf modellierte NQR-Übergangsfrequenzen, sowie Vorteile numerischer Implementierungen werden dargestellt und analysiert. Darüber hinaus wird ein neuartiger numerischer Fitting-Ansatz vorgestellt, der zwei NQR-Übergangsfrequenzen gleichzeitig berücksichtigt (vergrößerter Datensatz). Daraus gewonnene Fitting-Parameter bei Modellierung des Triphenylbismuth, wie Torsionsfrequenz und äquivalentes Trägheitsmoment von analytischen und numerischen Modellen sind vergleichbar und haben plausible Größenordnungen. Triphenylbismuth weist eine größere Temperatursensitivität als Tris(2-methoxyphenyl)bismuthine auf. Interessanterweise zeigten numerische Simulationen verschiedener Torsionsschwingungsrichtungen einen Einfluss auf das Vorzeichen des Temperaturkoeffizienten (niedrigste Übergangsfrequenz) unter Voraussetzung eines axial asymmetrischen elektrischen Feldgradienten. Abschließend werden wichtige Aspekte und Verbesserungen für zukünftige Modellierungsprozesse der Temperaturabhängigkeit von NQR-Übergangsfrequenzen vorgestellt.

Schlüsselwörter: NQRS, Triphenylbismuth, Tris(2-methoxyphenyl)bismuthine, Temperatursensitivität, Numerische Modellierung

Table of contents

1 Introduction

1.1 Motivation

The idea underlying this work originated during the collaboration in the FET-open project “CONQUER” funded by the European Commission. This multi-disciplinary project focused on the development of novel magnetic resonance imaging (MRI) contrast agents (CA´s) for molecular imaging (MI) **[1]**.
MRI is a tomographic imaging technique that generates images of the human body based on the water content and relaxation times of individual tissues. Contrast agents are molecules that are able to change the relaxation times and thus the image contrast in regions where the CA accumulates, e.g. tumors. In contrast to commercially available CAs (paramagnetic), this novel CA is based on cross-relaxation between protons and large quadrupolar nuclei and offers a variety of useful features **[1].**
In the course of this research Bi-aryl compounds proved to be promising in terms of their physical and chemical properties (tunability in NQR transition frequency, low toxicity, NQR transition frequency range applicable to clinical 1.5- and 3T MRI Systems) to enable quadrupole relaxation enhancement (QRE) **[2]**.
Of particular interest is the investigation of the temperature-dependent NQR transition frequency of Bi-aryl compounds and the underlying physical processes (molecular dynamics). Knowledge of Bi-aryl compound’s temperature sensitivity is of great importance, in order to predict the desired frequency crossing **[2]** of NQR transition frequencies and the Larmor frequency of protons at certain field strengths more precisely in the future. The modelling of temperature-dependent NQR transition frequencies will be the first step to gain such insights. Therefore, the focus of this thesis is set on numerical modelling to avoid simplifications caused by commonly used analytical models.

1.2 NQR Theoretical background

Nuclear quadrupole resonance spectroscopy (NQRS) is a technique methodically related to nuclear magnetic resonance spectroscopy (NMRS) that excites and finally detects transitions between discrete energy levels of the spin system due to an applied alternating magnetic field in the radiofrequency (RF) range. In contrast to NMR, the splitting of the sublevels of the "pure NQR" results from an interaction of the nuclear quadrupole moment with the electric field gradient (EFG), and not from an interaction of the magnetic dipole moment with a static magnetic field **[3]**, **[4]**.

1.2.1 Energy levels and the Hamiltonian

The interaction of the nucleus´s quadrupole moment Q with the associated electric field gradient ∇E causes a splitting of the nuclear ground state into different energy levels **[5]**.

The Hamiltonian of nuclear quadrupole interaction is described by the following tensor scalar product **[5]**:

$$H_Q = Q \cdot \nabla \mathrm{E} = \sum_m Q_2^m (\nabla \mathrm{E})_2^{-m} \tag{1.1}$$

With the irreducible components of the tensor Q,

$$\begin{aligned} Q_2^0 &= \frac{\mathrm{eQ}}{2I(2I-1)} (3\mathrm{I}_z^2 - \mathrm{I}^2) \\ Q_2^{\pm 1} &= \frac{\mathrm{eQ}}{2I(2I-1)} \frac{\sqrt{6}}{2} [\mathrm{I}_z (\mathrm{I}_x \pm \mathrm{iI}_y) + (\mathrm{I}_x \pm \mathrm{iI}_y)\mathrm{I}_z] \\ Q_2^{\pm 2} &= \frac{\sqrt{6}\mathrm{eQ}}{4I(2I-1)} (\mathrm{I}_x \pm \mathrm{iI}_y)^2 \end{aligned} \tag{1.2}$$

and tensor $\nabla \mathrm{E}$ **[5]**:

$$\begin{aligned} (\nabla \mathrm{E})_0 &= \frac{1}{2} \mathrm{V}_{zz} \\ (\nabla \mathrm{E})_{\pm 1} &= -\frac{1}{\sqrt{6}} (\mathrm{V}_{xz} \pm \mathrm{iV}_{yz}) \\ (\nabla \mathrm{E})_{\pm 2} &= \frac{1}{2\sqrt{6}} (\mathrm{V}_{xx} - \mathrm{V}_{yy} \pm 2\mathrm{iV}_{xy}) \end{aligned} \tag{1.3}$$

An easy to follow explanation/summary of the nuclear quadrupole moment Q and the electric field gradient ∇E (EFG) can be found in **[4]** resp. a more detailed one in **[3]**, **[5]**.

In the principal axis system (PAS) of the EFG **[3]**:

$$H_Q = \frac{e^2 qQ}{4I(2I-1)}[3I_z^2 - I^2 + \eta(I_x^2 - I_y^2)] \quad (1.4)$$

The rectangular brackets contain the angular momentum operators, while the $I's$ in the denominator correspond to the nuclear spin quantum number.
The quadrupole coupling constant e^2qQ (further named as Qcc) and the asymmetry parameter η are the basic quantities determined by nuclear quadrupole spectroscopy and contain information about the nuclear environment **[3]**.

"Do you know your Hamiltonian?"

Finding the right formulation of the Hamiltonian that describes the physical problem of interest is quite challenging. Fortunately, the Hamiltonian is known, but how does its parameters change with temperature?
Consequently, the main focus in this thesis is set to the development of the Hamiltonian´s parameters, precisely Qcc and η in terms of temperature and its numerical implementation, describing the NQR transition frequency temperature dependence in the observed molecular crystals of Triphenylbismuth and Tris(2-methoxyphenyl)bismuthine.

Within this master thesis the following key questions should be answered:

How do the Hamiltonian´s parameters change with temperature?
Which underlying physical model can describe this temperature dependency?
What are the advantages and disadvantages of numerical implementations concerning this physical problem?

The existing models describing NQR transition frequency temperature dependence typically use several approximations to end up with analytical expressions. This thesis aims to overcome the applied approximations and assumptions by using a numerical approach.

1.2.1.1 Energy levels in the case of axially symmetry

Axial symmetry $\eta = 0$ leads to a diagonalization of the Hamiltonian (represented in a so called “Zeeman basis”). This results in the following energy levels **[5]**:

$$\mathrm{E}_{\mathrm{Q}\pm\mathrm{m}} = \frac{Qcc}{4I(2I-1)}[3\mathrm{m}^2 - I(I+1)] \qquad (1.5)$$

The magnetic quantum number m can have the following $2I+1$ values $(-I, -I+1, \dots, I-1, I)$. The same energy level can be obtained by two quantum numbers which are identical in magnitude but different in sign (degenerate energy level). Nuclei with half-integer spin yield $I+1/2$ degenerate energy levels. An integer spin implies $I+1$ energy levels, of which I are degenerate **[5]**.

1.2.1.2 Energy levels in the case of axially asymmetry

For axially asymmetric electric field gradient $\eta > 0$, the energy levels can only be calculated analytically for spin 3/2 and spin 1 **[3]**.
Common practice is the evaluation of secular equations, which are used to obtain approximate solutions for the observed energy levels (see **[5]** page 12).
Furthermore, some numerical solutions can be found in the tables of Cohen ($I = \{\frac{9}{2}, \frac{7}{2}, \frac{5}{2}\}$) and Livingston/Zeldes ($I = \frac{5}{2}$) **[5]**.

1.2.2 Excitation of transitions between energy levels

By applying a magnetic RF field that interacts with the magnetic dipole moment of the nucleus, it is possible to excite transitions between different energy levels. The x- and y-components of the magnetic field allow quantum transitions between energy levels which differ by ± 1 in their magnetic quantum number m. If $\eta > 0$ also double quantum transitions $\Delta\mathrm{m} = \pm 2$ are allowed as shown in Figure 1.1 **[3]**, **[5]**.

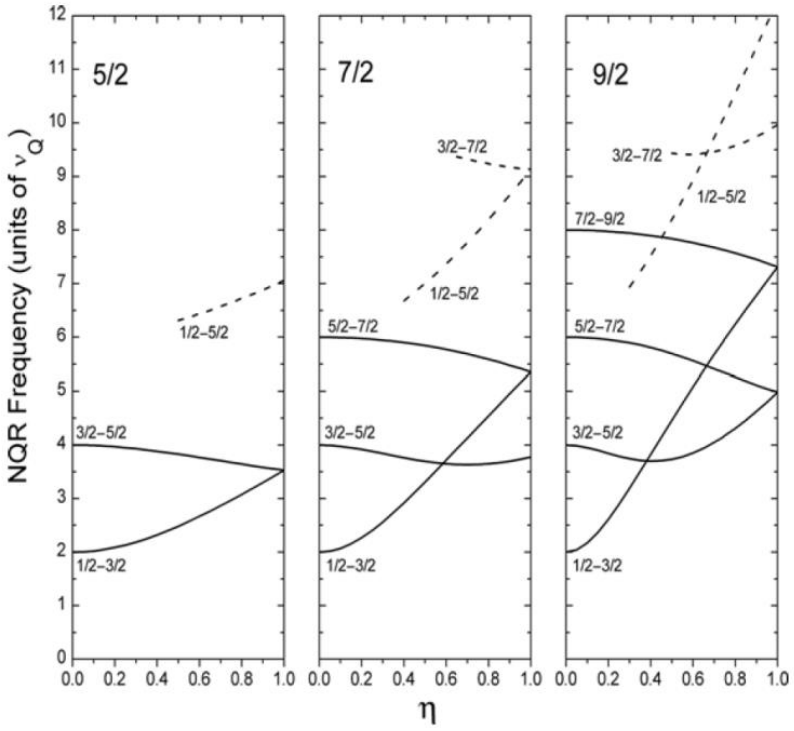

Figure 1.1: Shows possible transition frequencies with respect to η for spin 5/2, 7/2, and 9/2 nuclei reproduced from [3].

With suitable pulse-type RF-equipment **[6]**, **[7]** it is possible to measure these excited states and make possible NQR transition frequencies visible.

1.2.2.1 General definition of NQR transition frequency

The transition frequency is generally defined as follows **[5]**:

$$\nu_Q = \frac{E_{\pm m} - E_{\pm m-1}}{h} \qquad (1.6)$$

Equation (1.6) applies only to single quantum transitions.

In words, the energy difference is the transition frequency times h.

To achieve a significant transition probability between levels $\Delta \mathrm{m} = \pm 1$ resp. $\Delta \mathrm{m} = \pm 2$ for $\eta > 0$, the alternating RF-field frequency must be very close to the transition frequency (see **[8]** page 180).

1.3 Temperature dependence of NQR transition frequency

The following chapter explains the development of the most commonly used models to describe NQR transition frequency temperature dependence. Although the focus is set to molecular crystals, as it is the case for investigated Triphenylbismuth and Tris(2-methoxyphenyl)bismuthine.

1.3.1 The Bayer Model

Dehmelt and Krüger **[9]** were the first which reported a temperature dependence of NQR transition frequencies of crystal dichloroethylene resp. methylbromid. They assumed that molecular motions, precisely torsional oscillations, were responsible for the observed frequency shift with temperature.

Since torsional frequencies are much higher than the observed NQR transisition frequencies (>THz), the quadrupolar nucleus experiences a so called averaged electric field gradient (EFG). The magnitude of the effective electric field gradient seen by the quadrupolar nucleus is reduced, resulting in a decrease of the observed NQR transition frequency. The higher the temperature, the greater are the torsional amplitudes (torsional angles), which lead to a negative temperature coefficient of the NQR transition frequencies **[10]**.
The decrease of NQR transition frequencies with increasing temperature is the general case and is often reported in literature **[11]-[18]**.

However, there exist also few cases with positive temperature coefficients. Since their underlying physical interpretation is not the focus of this thesis, the reader is referred to **[19]**, **[20]** & **[21]**.
Bayer was the first who introduced a physical model to describe the temperature dependence of NQR transition frequency based on oscillatory torsional motions of the molecule, with the help of a quantum mechanical harmonic oscillator which relates the energy of the fluctuations to temperature **[10]**.

For Bayer´s model several assumptions are made [22]:

-The EFG tensor is axially symmetric ($\eta = 0$)
-The asymmetry parameter remains zero throughout the temperature range
-The oscillation is confined to a plane and takes place about the principal x- and y-direction of the EFG tensor
-The magnitude of the EFG tensor´s z-component remains unaltered during lattice oscillation
-The oscillations are assumed to be small $\{\theta(t) \ll 1\}$

The principal axes of the EFG tensor for the stationary molecule are defined as x, y and z (also defined as laboratory axis system (LABS) see section 2.3.1). According to Bayer **[10]** the molecule can execute oscillations about the x- and y-directions by torsional angles $\theta_x(t)$ and $\theta_y(t)$.
The time dependency of (harmonic) torsional oscillations can be described as follows **[10]**:

$$\theta(t) = \hat{\theta}(t)\sin(2\pi f_t t + \varphi(t)) \qquad (1.7)$$

With its torsional frequency f_t in Hz, peak amplitude of torsional angle $\hat{\theta}(t)$, time dependent torsional angle $\theta(t)$ and its statistical time dependent phase $\varphi(t)$.

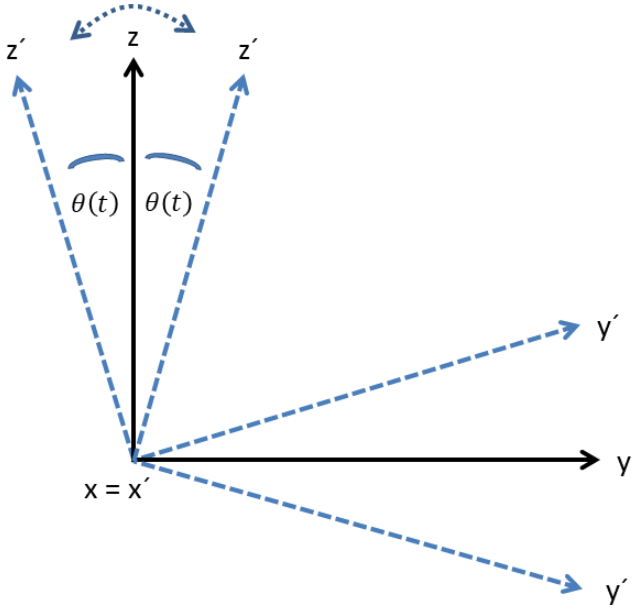

Figure 1.2: Torsional oscillation about the principal x-axis of the electric field gradient (EFG); x´, y´ and z´ determine the molecular fixed principle axis system

Under consideration of a harmonic oscillation, the mean $\langle\theta(t)\rangle$ resp. mean square $\langle\theta^2(t)\rangle$ of the time dependent torsional angle $\theta(t)$ can be written as follows,

$$\langle\theta(t)\rangle = 0 \text{ and } \langle\theta^2(t)\rangle = \frac{\widehat{\theta}^2(t)}{2} \tag{1.8}$$

The NQR transition frequency temperature dependence with respect to the mean square angle of the torsional oscillation can be described via (1.9) **[10]**,

$$\nu(T) = \nu_Q(1 - \frac{3}{2}\langle\theta^2(t)\rangle), \tag{1.9}$$

with $\nu_Q = \frac{Qcc}{2h}$ as the transition frequency of the stationary molecule in the case of spin I = 3/2.

Bayer **[10]** introduced the connection between torsional oscillations and temperature with the help of the quantum mechanical harmonic oscillator, by setting its mean energy in the thermodynamic equilibrium equal to the energy of a classic oscillator.

$$hf_t\left(\frac{1}{2} + \frac{1}{e^{\frac{hf_t}{kT}} - 1}\right) = 4\pi^2 {f_t}^2 A\langle\theta^2(t)\rangle, \tag{1.10}$$

where A is the moment of inertia of the molecule with respect to its torsional oscillation axis. A and f_t are parameters that can be related to molecule dynamics.

By considering the torsional oscillation about the x- and y-axis (formula) can be adapted by setting

$$\langle\theta^2(t)\rangle = \langle\theta_x^2(t)\rangle \; or \; \langle\theta_y^2(t)\rangle, \; f_t = f_{t,x} \; or \; f_{t,y} \text{ and } A = A_x \; or \; A_y \tag{1.11}$$

If the torsional oscillations occur independently about the x- and y-axis, $\langle\theta^2(t)\rangle$ can be expressed as $\langle\theta_x^2(t)\rangle + \langle\theta_y^2(t)\rangle$ **[22]**.

Substituting (1.10) in (1.9) finally yields the well-known Bayer equation **[10]**, **[22]**:

$$\nu(T) = \nu_Q[1 - \frac{3h}{8\pi^2}\sum_{i=x,y}\frac{1}{A_i f_{t,i}}\left(\frac{1}{2} + \frac{1}{e^{\frac{hf_{t,i}}{kT}}-1}\right)] \qquad (1.12)$$

Where ν_Q is the transition frequency of the stationary molecule (vibrationless lattice), depending on nuclear spin *I,* magnetic quantum number *m* and nuclear quadrupole coupling constant *Qcc (*as seen in **[23]** equation 12).

The transition frequency ν_0 at $T = 0K$ can be obtained with:

$$\nu_0 = \nu_Q[1 - \frac{3h}{16\pi^2}\sum_{i=x,y}\frac{1}{A_i f_{t,i}}] \qquad (1.13)$$

Bayers theory was verified qualitatively by many investigators and builds the basis for describing the NQR transition frequency temperature dependence related to torsional oscillations of the studied molecules, in molecular solids, resp. ionic solids **[5]**, **[11]** & **[12]**.
The harmonic oscillator model is valid only at low temperatures, or more precisely to temperatures far below the melting point of the samples studied. At higher temperatures approaching the melting point, the harmonic oscillator model no longer holds **[10]**, **[24]**.

1.3.2 Tatsuzaki Model

The original Bayer model assumes that the principal directions of the EFG tensor coincide with the principle directions of the moment of inertia tensor (harmonic torsional oscillation), which is not always the case **[17]**. Therefore Tatsuzaki and Yokozawa **[25]** introduced a correction term in Bayer´s equation to account for this **[22]**.

$$\nu(T) = \nu_Q[1 - \frac{3h}{8\pi^2}\sum_{i=x,y}\frac{sin^2\alpha_i}{A_i f_{t,i}}\left(\frac{1}{2} + \frac{1}{e^{\frac{hf_{t,i}}{kT}}-1}\right)] \qquad (1.14)$$

, with A_i as the moment of inertia, $f_{t,i}$ as the torsional oscillation about the i^{th} principal axis of the moment of inertia tensor. The angle between the principal z-axis of the EFG tensor and the i^{th} principal axis of the moment of inertia tensor is notated as α_i.

1.3.3 Kushida Model

Kushida generalized Bayer´s theory of motional averaging of the EFG, and considered all possible vibrational normal modes i of molecules in the crystal **[26]**. Further he rewrote (1.12) for the high temperature regime and low torsional frequencies ($\frac{hf_{t,i}}{kT} \ll 1$) with the help of following approximation **[26]**, **[22]**:

$$\frac{1}{2} + \frac{1}{e^x - 1} \cong \frac{1}{x} + \frac{x}{12} \tag{1.15}$$

to

$$\nu(T) = a\,(1 + bT + \frac{c}{T}) \tag{1.16}$$

where

$$a = \nu_Q = \frac{e^2 qQ}{2h}, \text{ in case of spin I = 3/2}$$

$$b = -\frac{3k}{8\pi^2}\sum_i \frac{1}{A_i f_{t,i}^2} \tag{1.17}$$

$$c = -\frac{h^2}{32\pi^2 k}\sum_i \frac{1}{A_i}$$

A_i corresponds to an equivalent moment of inertia of the i^{th} normal mode of molecular vibration.

Another important aspect, concerning modelling the NQR transition frequency temperature dependence, was introduced by Kushida, Benedek and Bloembergen **[23]**. They showed that the parameters a, b and c are functions of temperature as a result of thermal expansion (volume effects). Usually experiments are carried out at constant pressure conditions and not at constant volume conditions, so these parameters cannot be determined exactly from temperature measurements alone **[18]**. The constant volume assumption (1.16) leads consequently to a mismatch between measured and modeled NQR transition frequency data, especially in the high temperature regime.
An adequate analysis of the NQR transition frequency temperature dependence with Kushidas theory (1.16) can only be achieved when the NQR transition frequency is known as a function of volume for a series of different temperatures **[23]**.

1.3.4 Brown Model

Kushida, Benedek and Bloembergen **[23]** assumed that the torsional frequency $f_{t,i}$, the equivalent moment of inertia A_i and the NQR transition frequency for the stationary molecule ν_Q are volume dependent.

For molecular crystals, like the samples considered in this Thesis the following simplifications can be assumed:

-The transition frequency of the stationary molecule ν_Q is approximately independent of volume due to small volume dependent contributions of lattice fields to the quadrupole coupling constant.
-The equivalent moment of inertia A_i, which can be calculated from molecular dimensions alone, will also be assumed to be independent of volume **[27]**.

Both simplifications are possible, due to the fact that in molecular crystals, the change in bond lengths and bond angles with temperature are negligible **[22]**.

The remaining volume dependence of the torsional frequency $f_{t,i}$ can be introduced with the help of a linear model **[27]**, which is based on temperature dependent measurements of low frequency Raman lines by Ichishima **[28]**:

$$f_{t,i} = f_{t,i0}(1 - g_i \Delta t) \qquad (1.18)$$

Where $f_{t,i}$ is the value of the torsional frequency at any fixed temperature $\Delta t = T - T_0$, at temperature $\Delta t = 0K$ follows, $f_{t,i} = f_{t,i0}$, and g_i is the so-called temperature coefficient of the torsional frequency **[27] [22]**.

Such linear relationship agrees well with the measurements on naphthalene made by Ichishima **[28] [22]**.
In view of this relationship for the temperature dependence of $f_{t,i}$, constant b in Kushida´s formula (1.16) becomes also temperature dependent. This circumstance leads to a non-linear temperature dependence of the NQR transition frequency under constant pressure conditions **[27]**.

Brown introduced the following method to obtain a value for the temperature coefficient of the torsional frequency g_i **[27]**:

At first it is assumed that g_i of all vibrational modes i are equal,

$$\langle g_i \rangle = \ g \ and \ \langle {g_i}^2 \rangle = \langle g_i \rangle^2 = \ g^2 \tag{1.19}$$

Followed by skipping the term $\frac{c}{T}$ from (1.16) (which holds for large moments of inertia and relatively high temperatures) and taking the first and second derivatives, obtaining a pair of equations **[27]**, **[22]**:

$$\begin{aligned} \frac{1}{\nu_Q}\frac{dv}{dt}\bigg|_{T_0} &= (1 + 2T_0 g)b_0 \\ \frac{1}{\nu_Q}\frac{d^2v}{dt^2}\bigg|_{T_0} &= (4g + 6T_0 g^2)b_0 \end{aligned} \tag{1.20}$$

with the weighted averages $\langle g_i \rangle$ and $\langle g_i \rangle^2$,

$$\begin{aligned} \langle g_i \rangle &= \frac{\sum_i (\frac{1}{A_i f_{t,i0}^2}) g_i}{\sum_i (\frac{1}{A_i f_{t,i0}^2})} \\ \langle g_i \rangle^2 &= \frac{\sum_i (\frac{1}{A_i f_{t,i0}^2}) {g_i}^2}{\sum_i (\frac{1}{A_i f_{t,i0}^2})} \end{aligned} \tag{1.21}$$

Whereby b_0 (value of b at $\Delta t = 0K$) and g are obtained by solving this pair of equations (1.20) at any convenient high temperature reference point T_0!
For evaluating the derivatives at the reference point, it has been normal practice to fit the measurement data to a parabola **[17]**, **[18]**, **[29]** & **[30]**.

Brown observed that the introduction of the temperature-dependent torsional frequency term (1.18) represents a good agreement between the theoretically and experimentally determined value of b_0 in p-dichlorobenzene **[27]**, **[22]**.

The models mentioned so far refer directly to the change of the measurable NQR transition frequency with temperature. Though, the temperature-dependent change of the Hamiltonian´s parameters, namely Qcc and η are introduced and analyzed in detail in the methods chapter.

1.3.5 Normal Modes

Above assumption of torsional oscillation´s of the electric field gradient is based on vibrations of molecules in the crystal lattice. These vibrations, more precisely sinusoidal oscillations, can be described in the form of normal modes with defined frequencies *f*. Thus, a general motion can be described as a superposition of independent (orthogonal) normal modes. The number of possible normal modes in a molecule depends on the total number of degrees of freedom (3N for N atoms) and can be categorized by the type of motion like wagging, stretching, torsion etc. **[31]**.

Energy of normal modes:

The energy levels E_n of a vibrational mode with vibrational frequency f (harmonic oscillator approximation) is given by:

$$E_n = hf\left(n + \frac{1}{2}\right), \qquad (1.22)$$

where n are integers defining the different energy levels and hf is the energy quanta needed to make transitions between these energy levels possible **[32]**. Transitions between different energy levels (rotational, vibrational), so called optical modes can be detected by means of Raman and/or Infrared (IR) spectroscopy.

2 Methods

This chapter introduces the practical implementation concerning the NQR transition frequency temperature dependency of the investigated molecular crystals Triphenylbismuth and Tris(2-methoxyphenyl)bismuthine. First, the observed molecular crystals and their data sets to be analyzed are described, followed by a detailed explanation of the modelling methods and numerical implementations used.

2.1 Observed molecules and measurement data

In the course of the FET-open project “CONQUER” Bi-aryl compounds, like Triphenylbismuth (further termed as BIPH3) and Tris(2-methoxyphenyl)bismuthine (further termed as BIPH3_OME) proved to be promising in terms of their physical and chemical properties: NQR transition frequency range applicable to clinical 1.5- and 3T MRI systems, low toxicity and tunability in frequency by chemical modification **[2]**. Therefore, all modelling processes in this thesis focused on these two substances. The following section shows their chemical, physical (Table 2.1) and NQR properties (Table 2.2) together with a description of the observed measurement data (Table 2.3).

2.1.1 Triphenylbismuth and Tris(2-methoxyphenyl)bismuthine

Table 2.1: Chemical and physical properties of BIPH3 and BIPH3_OME [33]

Synonyms	Molecular formula	Appearance	Molecular weight in g/mol	Melting point in °C	Type of crystalline solid
Triphenylbismuthine, BIPH3*	$C_{18}H_{15}Bi$	Light yellow powder	440.29	76-81	Molecular solid
Tris(2-methoxyphenyl)-bismuthane BIPH3_OME*	$C_{21}H_{21}BiO_3$	Solid	530.37	162-165	Molecular solid

*…labeling in this thesis

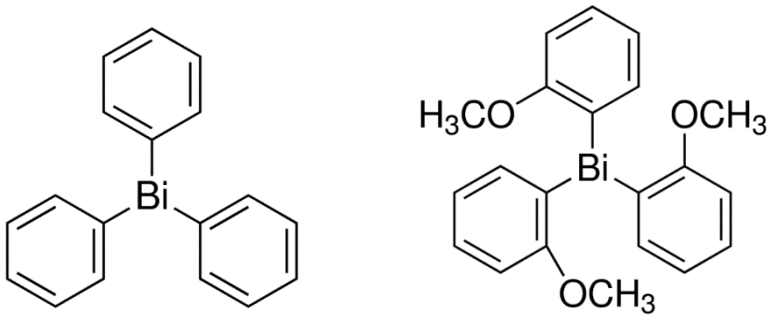

Figure 2.1: 2D-Structure of BIPH3 and BIPH3_OME [33]

NQR properties

$^{209}_{83}Bi$, with a nuclear spin quantum number of *I = 9/2* is the quadrupolar nucleus (QN) of interest. The interaction of its quadrupole moment with the electric field gradient gives rise to 10 energy levels and 4 pure (no external magnetic field applied) NQR transition frequencies (single quantum transitions that are further named as Transition 1...4 according to frequency in ascending order). All originating pure NQR transition frequencies can be completely described by means of the quadrupole coupling constant Qcc and the asymmetry parameter η.

Table 2.2: NQR properties of BIPH3 and BIPH3_OME [2]

Sample name	Temperature in K	Qcc in MHz	η (1)
BIPH3	310	668.9	0.083
	77	684.6	0.090
BIPH3_OME Site A	310	715.2	0.000
	77	n/a.	n/a.
BIPH3_OME Site B	310	714.3	0.000
	77	n/a.	n/a.

n/a…no measurement data available

Table 2.2 lists the quadrupole coupling constant Qcc and the asymmetry parameter η of BIPH3 and BIPH3_OME at two different temperatures.

BIPH3´s quadrupole coupling constant shows a clear temperature dependency (negative temperature coefficient), whereas for BIPH3_OME only data at 310K was available so far. Furthermore BIPH3_OME has two crystallographic inequivalent sites, resulting in slightly different quadrupole coupling constants. The asymmetry parameters of both substances are relatively small or even zero. Therefore, it´s common to assume axially symmetric field gradients of BIPH3 and BIPH3_OME.

2.1.2 Measurement data

All measurement data were obtained using a self-built wideband pulse-type NQR spectrometer (50 - 150 MHz) developed at the Institute of Medical Engineering **[6]**, **[7]**. With the help of a cryostatic wideband probehead **[34]** combined with a liquid nitrogen (LN) flow cryostat, measurements of NQR transition frequencies (Transition 3 and Transition 4) of BIPH3 and BIPH3_OME at several temperatures were possible (Range from -196 °C/77.15 K to 50 °C/323.15 K). Transition 3 resp. 4 denotes the $\pm 5/2 \leftrightarrow \pm 7/2$ resp. $\pm 7/2 \leftrightarrow \pm 9/2$ transitions. All measurements were performed as part of Felix Theyer´s bachelor thesis. The thesis contains a detailed description of the measurement setup and methods used **[35]**.

Table 2.3 : Measured NQR transition frequencies with error estimation $\Delta\nu(T_0)$ of BIPH3 and BIPH3_OME

	BIPH3		BIPH3_OME Site A	
Temperature T_0 in K	**Transition 3 ± $\Delta\nu(T_0)$ in MHz**	**Transition 4 ± $\Delta\nu(T_0)$ in MHz**	**Transition 3 ± $\Delta\nu(T_0)$ in MHz**	**Transition 4 ± $\Delta\nu(T_0)$ in MHz**
77.15	85.44 ± 0.01	114.03 ± 0.02	n/a.	n/a.
133.15	85.17 ± 0.02	113.65 ± 0.03	n/a.	n/a.
153.15	85.04 ± 0.02	113.48 ± 0.03	90.06 ± 0.03	120.10 ± 0.03
173.15	84.89 ± 0.02	113.23 ± 0.03	90.01 ± 0.03	120.04 ± 0.03
193.15	84.68 ± 0.03	113.01 ± 0.03	89.95 ± 0.03	119.93 ± 0.03
213.15	84.51 ± 0.03	112.78 ± 0.04	89.89 ± 0.03	119.82 ± 0.04
233.15	84.41 ± 0.03	112.65 ± 0.04	89.83 ± 0.04	119.77 ± 0.04
253.15	84.17 ± 0.04	112.32 ± 0.06	89.67 ± 0.05	119.59 ± 0.05
273.15	83.90 ± 0.05	111.65 ± 0.06	89.63 ± 0.05	119.56 ± 0.06
293.15	83.59 ± 0.05	111.55 ± 0.07	89.47 ± 0.05	119.29 ± 0.06
313.15	83.35 ± 0.05	111.21 ± 0.07	89.29 ± 0.06	119.02 ± 0.07
323.15	83.22 ± 0.06	111.05 ± 0.07	89.16 ± 0.06	118.90 ± 0.07

n/a…no measurement data available

Table 2.3 shows the determined maxima of the measured spectra together with its calculated error estimation using equation 2.1. The analysis of BIPH3_OME´s Site B is not part of this work due to lack of valid data.

Error estimation of measurement data

Numerous factors influenced the accuracy of the measurement results, such as thermocouple placement, frequency resolution of the acquired NQR spectra or stability of the temperature control. In order to take these influences into account, the following error estimation was applied, which is based on the error estimation in **[35]**.

Equation 2.1 introduces the applied error estimation with respect to the measured NQR transition frequency,

$$\Delta\nu(T_0) = \left|\frac{d\nu}{dT}\right|_{T_0} \Delta T_0 + \Delta\nu_{spec}/2 \qquad (2.1)$$

Where $\Delta\nu(T_0)$ is the magnitude of the NQR transition frequency´s error estimation (precisely, positive and negative value of error bar), $\left.\frac{d\nu}{dT}\right|_{T_0}$ is the temperature coefficient at the evaluated temperature T_0, ΔT_0 is its estimated deviation and $\Delta\nu_{spec}$ is the frequency resolution of the measured NQR spectra. A generous temperature deviation of $\Delta T_0 = 2.5$ K resp. 3.5 K was chosen for measurement points in the ranges [77.15 K …233.15 K] resp. [253.15 K...323.15 K]. The obtained NQR transition frequency resolution $\Delta\nu_{spec}$ equals 10 kHz for BIPH3 and 50 kHz for BIPH3_OME regarding the used sequence (acquisition window) in **[35]**.
The influence of a Lorentz fit on the measurement accuracy/error was negligible, so the measured maximum values (Table 2.3) of the NQR transition frequencies were selected for all further analyses.

2.2 Fitting Models

The following section presents the adaption of the used fitting models describing the NQR transition frequency temperature dependency of BIPH3 and BIPH3_OME.
This step provides a quick check of the underlying physical model used, before the focus can be set on a purely numerical implementation.

Regarding molecular crystals, two simplifications (section 1.3.4) of Kushida´s model (1.16) are possible, leading to the used Kushida-Brown model. The adaption of the Kushida-Brown model for our purposes and its application to the measurement data is described below.

Fitting equation for high temperature regime (Kushida-Brown-Model)

Kushida's formula (1.16 and 1.17) for the high temperature regime is recalled,

$$\nu(T) = a\,(1 + bT + \frac{c}{T}) \tag{1.16}$$

where,

$$a = \nu_Q = \frac{e^2qQ}{2h}, \text{ in case of spin } I = 3/2$$

$$b = -\frac{3k}{8\pi^2}\sum_i \frac{1}{A_i f_{t,i}^2} \tag{1.17}$$

$$c = -\frac{h^2}{32\pi^2 k}\sum_i \frac{1}{A_i}$$

For simplifications only one vibrational mode i is assumed.
Replacing the sum in b and c and substituting constant terms with $b´$ and $c´$ leads to the following result:

$$a = \nu_Q;\ b´ = -\frac{3k}{8\pi^2};\ c´ = -\frac{h^2}{32\pi^2 k} \tag{2.2}$$

with,

$$b = b' \frac{1}{A f_t^2}$$
$$c = c' \frac{1}{A} \tag{2.3}$$

Since the fitting parameter $a = \nu_Q$ depends on spin *I* and magnetic quantum number *m*, it is different for each spin *I* and transition.

Furthermore, replacement of the torsional frequency f_t with Brown´s linear model $f_t = f_{t,0}(1 - g\Delta t)$ (1.18) to take volume dependency into account.

In a final step, g must be calculated from the measurement data: Therefore, Brown´s method (1.19 – 1.21) is applied to the measurement data,

$$\frac{1}{\nu_Q}\frac{dv}{dt}\bigg|_{T_0} = (1 + 2T_0 g)b_0$$
$$\frac{1}{\nu_Q}\frac{d^2v}{dt^2}\bigg|_{T_0} = (4g + 6T_0 g^2)b_0 \tag{2.4}$$

The evaluation of the derivatives at the reference point $T_0 = 293.15K$ was done by fitting a polynomial of 2nd order to the measurement data. These values were obtained using the MATLAB solvers **polyfit** and **polyder**.

Building the ratios of the above equations (2.4) skips the parameters ν_Q and b_0,

$$r_d = \frac{\frac{dv}{dt}\big|_{T_0}}{\frac{d^2v}{dt^2}\big|_{T_0}} = \frac{1+2T_0 g}{4g+6T_0 g^2} \tag{2.5}$$

Equation (2.5) can be rewritten to the following quadratic equation:

$$(4r_d - 2T_0)g + 6r_d T_0 g^2 - 1 = 0$$
$$xg^2 + yg + z = 0 \tag{2.6}$$

Where,

$$x = 6r_d T_0$$
$$y = 4r_d - 2T_0$$
$$z = -1$$

The quadratic equation (2.6) was solved with the MATLAB solver **roots**. It gives two results for g, where only the positive value was used.

Finally, the adapted Kushida-Brown´s fitting equation for the high temperature regime (2.7) can be written as follows:

$$\nu(T) = \nu_Q \left(1 + b' \frac{1}{A f_{t,0}^2 [1 - g(T - T_0)]^2} T + c' \frac{1}{AT}\right), \qquad (2.7)$$

where b', c' and g are known constants, and ν_Q, A resp. $f_{t,0}$ are the unknown fitting parameters.

Fitting equation without high temperature approximation (Bayer-Brown-Model)

To get rid of the high temperature approximation it is possible to use Bayer´s formulation (1.12).
Adapted to only one vibrational mode i and under consideration of a volume dependent torsional frequency f_t, equation (1.12) results in:

$$\nu(T) = \nu_Q \left[1 - \frac{3h}{8\pi^2} \frac{1}{A f_{t,0} [1 - g(T - T_0)]} \left(\frac{1}{2} + \frac{1}{e^{\frac{h f_{t,0} [1 - g(T - T_0)]}{kT}} - 1}\right)\right] \qquad (2.8)$$

The torsional frequency´s temperature coefficient g can be obtained the same as described above with Brown´s method.

Application of the adapted fitting models to the measurement data

The fitting equations (2.7 and 2.8) were applied separately to our given measurement data (section 2.1.2). A comparison of the models shows the influence of the high temperature approximation in the low temperature regime.

The nonlinear least square solver used was **lsqnonlin** and executed a trust-region-reflective algorithm. As termination tolerance **'TolFun'** was set to 1e-10. Additionally, **'MaxIter'** resp. **'MaxFunEvals'** was set to 1000 and 1500.

The initial parameters and boundary conditions were defined as follows:

Table 2.4: Initial parameters and boundary conditions of fitting models

	$f_{t,0}\ in\ THz$	$A\ in\ 10^{-44} in\ kgm^2$	$\nu_Q\ in\ MHz$ Transition 3/Transition 4
BIPH3			
Initial parameters	1	1	85.55/114.26
Lower bounds	0	0	0
Upper bounds	100	100	200
BIPH3_OME			
Initial parameters	1	1	89.61/119.45
Lower bounds	0	0	0
Upper bounds	100	100	200

10^{-44}, 10^{12} and 10^{6} are scaling factors to avoid too small/large numerical values during the fitting procedure. The initial parameter ν_Q was determined using the evaluation of the polynomial fit of 2nd order at 0 K.
The parameters obtained in these fittings and their goodness of fit are presented in chapter results (Table 3.2).

2.3 Numerical implementations

As already described in chapter 1.3, torsional oscillations of our investigated molecules seem to be mostly responsible for the temperature-dependent change of the NQR transition frequency. This chapter focuses on the numerical implementation and evaluation of this physical model.
The first part deals with different formulations of the nuclear quadrupole interaction Hamiltonian (recall section 1.2.1) and their evaluation to obtain the NQR-transition frequencies of interest.
The temperature dependency of NQR transition frequencies resp. their underlying nuclear quadrupole interaction Hamiltonian's parameters due to torsional oscillations is introduced in section 2.3.2. First, an analytical model is presented that describes the temperature-dependent variation of the nuclear quadrupole coupling constant Qcc and the asymmetry parameter η. Followed by a numerical implementation of the nuclear quadrupole interaction Hamiltonian´s motional averaging, also leading to a change of Qcc and η. Furthermore, the calculation of Qcc and η from two NQR transition frequencies, precisely Transition 3 and Transition 4, is described. In addition, the numerical implementations obtained are tested and compared with the help of the fitting parameters acquired in section 2.2. Finally, a novel numerical fitting approach is introduced and tested with the measurement data.

The entire implementation process was carried out in **MATLAB** (MathWorks).

2.3.1 Hamiltonian of nuclear quadrupole interaction - different representations

Numerical implementation of the nuclear quadrupole interaction Hamiltonian is an essential part in this thesis, therefore 3 slightly different numerical approaches of the nuclear quadrupole Hamiltonian are introduced. In addition, the numerical evaluation of the introduced Hamiltonians, to get finally the wanted NQR transition frequencies, is described in detail.

2.3.1.1 Hamiltonian in the principle axis system and its eigenvalue problem

Commonly used is the formulation of the Hamiltonian in the principle axis system of the electric field gradient (1.4). In the principle axis system, the real symmetric traceless 3x3 EFG-tensor reduces to three components, namely V_{xx}, V_{yy} and V_{zz}.
Therefore, the electric field gradient is completely characterized by two parameters: $eq = V_{zz}$ the z-component of the electric field gradient, which is part of $Qcc = e^2qQ$ and the already known $\eta = \frac{V_{xx}-V_{yy}}{V_{zz}}$.
η can take values between 0 and 1, whereby condition $|V_{xx}| \leq |V_{yy}| \leq |V_{zz}|$ in the principle axis system must be satisfied **[3]**.

The following steps were carried out to obtain the wanted NQR transition frequencies:

Hamiltonian: Matrix representation

Recall equation 1.4:

$$H_Q = \frac{Qcc}{4I(2I-1)}[3\mathrm{I}_z^2 - \mathrm{I}^2 + \eta(\mathrm{I}_x^2 - \mathrm{I}_y^2)] \qquad (1.4)$$

Where Qcc, η and I are all scalar values.
Although, the spin operator I and its components $\mathrm{I_x}$, $\mathrm{I_y}$ and $\mathrm{I_z}$ in the square bracket ($\mathrm{I} = (\mathrm{I_x},\ \mathrm{I_y},\ \mathrm{I_z})$, where $\mathrm{I}^2 = \mathrm{I}_x^2 + \mathrm{I}_y^2 + \mathrm{I}_z^2$) have to be represented in matrices by selecting a suitable base (Zeeman base) to make further analysis possible.

For a nuclear spin quantum number I above-mentioned spin operators can be described as square matrices of dimension $2I+1$. More precisely, they are represented in the Zeeman basis with states* $|m\rangle$ (where m is the magnetic quantum number) that satisfy the following conditions **[36]**:

$$\begin{gathered}
\langle m'|\mathrm{I_x}|m\rangle = \left(\delta_{m',m+1} + \delta_{m+1',m}\right)\frac{1}{2}\sqrt{I(I+1) - m'm} \\
\langle m'|\mathrm{I}_y|m\rangle = \left(\delta_{m',m+1} - \delta_{m+1',m}\right)\frac{1}{2i}\sqrt{I(I+1) - m'm} \\
\langle m'|\mathrm{I}_z|m\rangle = \delta_{m',m}m \\
\langle m'|\mathrm{I}_+|m\rangle = \delta_{m',m+1}\sqrt{I(I+1) - m'm} \\
\langle m'|\mathrm{I}_-|m\rangle = \delta_{m'+1,m}\sqrt{I(I+1) - m'm} \\
\langle m'|\mathrm{I}^2|m\rangle = \delta_{m',m}I(I+1)
\end{gathered} \tag{2.9}$$

Where $\delta_{i,j}$ is generally known as the Kronecker-Delta:

$$\delta_{i,j} = \begin{cases} 1, & i = j \\ 0, & i \neq j \end{cases} \tag{2.10}$$

I_+ and I_- in 2.11 are the non-Hermitian ladder operators **[36]**:

$$\mathrm{I}_+ = \mathrm{I_x} + i\mathrm{I}_y \text{ and } \mathrm{I}_- = \mathrm{I_x} - i\mathrm{I}_y \tag{2.11}$$

Thus, for a nuclear spin quantum number of *I* = 9/2, like the investigated $^{209}_{83}Bi$, the spin operators are represented in 10x10 matrices with 10 eigenstates (Zeeman basis):

$$|-9/2\rangle, |-7/2\rangle, |-5/2\rangle, |-3/2\rangle, |-1/2\rangle, |1/2\rangle, |3/2\rangle, |5/2\rangle, |7/2\rangle, |9/2\rangle$$

To calculate the required matrices for different nuclear spin quantum numbers *I*, a MATLAB function *spinmat(I)* with the above-mentioned conditions (2.9) was written. By applying function *spinmat(I)* to *I* = 9/2, it was possible to calculate all matrices needed for the evaluation of equation 1.4.

*Detailed information regarding quantum mechanical states (eigenstates and eigenvalues), quantum mechanical operators as well as the formulation of the eigenvalue problem of linear Hermitian operators (observables), can be found in (**[37]** p.134 & p.159).

Solving the eigenvalue problem

The first step was required to obtain the nuclear quadrupole interaction Hamiltonian in its matrix representation. Finally, the NQR transition frequencies $\nu_Q = \frac{E_{\pm m} - E_{\pm m-1}}{h}$, which are defined as the difference between two energy levels divided by h, must be calculated from the given Hamiltonian.

In quantum mechanics the Hamiltonian is also known as the „Energy-Operator“ **[8]**. Its unknown energy-levels $E_{\pm m}$ (eigenvalues) and eigenstates (eigenvectors) $|\varphi\rangle$ can be obtained by solving the following eigenvalue problem (2.12) **[37]**:

$$H_Q|\varphi\rangle = E|\varphi\rangle \qquad (2.12)$$

Eigenvalue problem in the case of axial symmetry

As shown in section 1.2.1.1, axially symmetry $\eta = 0$ leads to a diagonalization of the Hamilton matrix (represented in the Zeeman basis). Consequently, the eigenvalues searched for are easy to obtain, since they are placed on the principal diagonal.
The desired NQR transition frequency can be easily determined by evaluating the difference between the energy levels of interest.
For example, $\frac{E_{\pm 9/2} - E_{\pm 7/2}}{h}$ gives NQR Transition 4 (*I* = 9/2).
In the case of axial symmetry the calculated eigenstates match the previously mentioned Zeeman states $|\varphi\rangle = |m\rangle$.

Eigenvalue problem in the case of axial asymmetry

Generally, the EFG deviates from axially symmetry $\eta \neq 0$ resulting in a nondiagonal Hamilton matrix. In that case the eigenvalues have to be obtained by diagonalizing the given Hamilton matrix $D_{HQ} = U^+ H_Q U$. The columns of the unitary transformation matrices ($U^+ U = 1$) contain the eigenvectors of H_Q **[37]**. Diagonalization leads to a change of the basis, more precisely the calculated eigenstates $|\varphi\rangle$ are now linear combinations of Zeeman states $|\mathrm{m}\rangle$.
Common numerical methods solving eigenvalue problems are the Cholesky factorization or the generalized Schur decomposition (QZ algorithm).
In the course of this thesis the MATLAB solver ***eig*** was applied to all occurring eigenvalue problems. The MATLAB implementation chooses therefore between the

Cholesky factorization and the QZ algorithm, regarding the given matrix properties (symmetry, Hermitian) **[38]**.

2.3.1.2 Bayer Approach

Bayer was the first who introduced an angle dependency $\theta(t)$ of the nuclear quadrupole Hamiltonian to account for the observed molecule's torsional oscillation **[10]**. For reasons of simplicity ($\eta = 0$), he assumed only one torsional oscillation, occurring about the y-principal axis of the EFG **[10]**.

The principle axis system of the stationary molecule (x, y, z; also called laboratory axis system LABS) has to be related to the molecular fixed principle axis system (x´, y´, z´).

The EFG components in the laboratory axis system (LABS) are described by the following equations:

$$\begin{aligned} V_{zz} &= \tfrac{1}{2}V_{z'z'}\left(3cos^2\left(\theta(t)\right)-1\right) \approx V_{z'z'}\left(1-\tfrac{3}{2}\,\theta^2(t)\right), whereby\ \theta(t) \ll 1 \\ V_{xx} &= \tfrac{1}{2}V_{z'z'}\left(3sin^2\left(\theta(t)\right)-1\right) \approx V_{z'z'}\left(\tfrac{3}{2}\,\theta^2(t)-\tfrac{1}{2}\right), whereby\ \theta(t) \ll 1 \\ V_{xz} &= -\frac{3}{2}V_{z'z'}sin(\theta(t))\cos(\theta(t)) \approx -\frac{3}{4}V_{z'z'}\theta(t), whereby\ \theta(t) \ll 1 \\ & V_{yy} = -\tfrac{1}{2}V_{z'z'},\ V_{yz} = V_{xy} = 0 \end{aligned} \qquad (2.13)$$

Here, the tensor component V_{xz} is not zero as in the PAS case.

Thus, the Bayer Hamiltonian of the nuclear quadrupole interaction in the LABS can be formulated as follows:

$$H_Q = \frac{eQ}{2I(2I-1)}\left[V_{xx}\mathrm{I}_\mathrm{x}^2 + V_{yy}\mathrm{I}_\mathrm{y}^2 + V_{zz}\mathrm{I}_\mathrm{z}^2 + V_{xz}(\mathrm{I}_\mathrm{x}\mathrm{I}_\mathrm{z} + \mathrm{I}_\mathrm{z}\mathrm{I}_\mathrm{x})\right] \qquad (2.14)$$

With sufficiently small angles $\theta(t) \ll 1$ the approximated Bayer Hamiltonian is given by:

$$H_Q = \frac{1}{8}\frac{eQV_{z'z'}}{I(2I-1)}\Big[(6\mathrm{I}_z^2 - 2\mathrm{I}^2)\left(1 - \frac{3}{2}\,\theta^2(t)\right) - 3\theta(t)[\,(\mathrm{I}_+ + \mathrm{I}_-)\mathrm{I}_z + \mathrm{I}_z(\mathrm{I}_+ + \mathrm{I}_-)] + \frac{3}{2}\,\theta^2(t)(\mathrm{I}^2{}_+ + \mathrm{I}^2{}_-)\Big] \qquad (2.15)$$

The first term contains the Hamiltonian (for $\eta = 0$) with the perturbation caused by torsional oscillations, followed by terms containing ladder operators.
The next section illustrates a more general formulation, that considers torsional oscillations occurring around all three coordinate axes!

2.3.1.3 Hamiltonian in the laboratory axis system

In order to allow oscillations of the investigated molecule about an arbitrary axis, the representation of the Bayer Hamiltonian must be adapted. With the help of Euler angles (α, β, γ) it is possible to describe the orientation of the molecule (precisely its EFG tensor) in the three-dimensional laboratory axis system (LABS).
As in the previous case, the principle axis system and the laboratory axis system of the EFG tensor must be related to each other.

The EFG tensor in the LAB system under consideration of Euler angles (α, β, γ) is given by **[39]**, **[40]**:

$$V_{2,0} = \frac{eq}{2}\left[\frac{3\cos^2(\beta)-1}{2} + \eta\,\frac{\sin^2(\beta)(e^{2i\gamma}+e^{-2i\gamma}}{4}\right]$$

$$V_{2,\pm1} = \frac{eq}{2}\left[\mp\sqrt{\frac{3}{8}}\sin(2\beta)\,e^{\pm i\alpha} + \frac{\eta}{\sqrt{6}}\left(-\frac{1\mp\cos(\beta)}{2}\sin(\beta)\,e^{\pm i(\alpha\mp 2\gamma)} + \frac{1\mp\cos(\beta)}{2}\sin(\beta)e^{i(\pm\alpha+2\gamma)}\right)\right]$$

$$V_{2,\pm2} = \frac{eq}{2}\left[\mp\sqrt{\frac{3}{8}}\sin^2(\beta)\,e^{\pm 2i\alpha} + \frac{\eta}{\sqrt{6}}\left(\frac{(1\mp\cos(\beta))^2}{4}e^{\pm 2i(\alpha\mp\gamma)} + \frac{(1\pm\cos(\beta))^2}{4}e^{2i(\pm\alpha+\gamma)}\right)\right] \qquad (2.16)$$

The above representation results using Wigner-D matrix elements **[39]**

With the help of the above introduced EFG tensor (2.16) a general formulation of the nuclear quadrupole interaction Hamiltonian in the LAB system is possible **[39]**, **[40]**:

$$H_Q = \frac{eQ}{I(2I-1)}\left[\frac{1}{2}(3\mathrm{I}_z^2 - \mathrm{I}^2)\mathrm{V}_{2,0} + \frac{\sqrt{6}}{4}\Big((\mathrm{I}_z\mathrm{I}_+ + \mathrm{I}_+\mathrm{I}_z)\mathrm{V}_{2,-1} - (\mathrm{I}_z\mathrm{I}_- + \mathrm{I}_-\mathrm{I}_z)\mathrm{V}_{2,+1} + \mathrm{I}^2{}_+\mathrm{V}_{2,-2} + \mathrm{I}^2{}_-\mathrm{V}_{2,+2}\Big)\right] \quad (2.17)$$

The above formulation permits the EFG tensor to be rotated in arbitrary directions without assuming an axially symmetric EFG ($\eta \neq 0$).
Therefore, this formula will be our preferred choice when simulating torsional oscillations and the resulting averaging of the electric field gradient.

2.3.2 Averaging of Hamiltonian

The temperature-dependent change of the NQR transition frequency was discussed in detail in the introduction. In this section the temperature-dependent change of the associated nuclear quadrupole interaction Hamiltonian's parameters is presented.
Thus, methods for the simulation of the EFG's motional averaging, caused by temperature-dependent torsional oscillations of the investigated molecules, are introduced.
To give insight into the temperature-dependent change of the Hamiltonian's parameters, a common analytical approach is presented first, followed by a novel numerical implementation.

Recall torsional oscillation:

The time-dependency of (harmonic) torsional oscillations were introduced with the help of the following equation (1.7) **[10]**:

$$\theta(t) = \hat{\theta}(t)\sin(2\pi f_t t + \varphi(t)) \qquad (1.7)$$

Under consideration of a harmonic oscillation, the mean $\langle\theta(t)\rangle$ resp. mean square $\langle\theta^2(t)\rangle$ of the time-dependent torsional angle $\theta(t)$ have the following values (1.8):

$$\langle\theta(t)\rangle = 0 \text{ and } \langle\theta^2(t)\rangle = \frac{\hat{\theta}^2(t)}{2} \qquad (1.8)$$

The mean of the time-dependent torsional angle equals zero $\langle\theta(t)\rangle = 0$, in the case of harmonic oscillations.

2.3.2.1 Analytical averaging of Hamiltonian

Harmonic oscillations cause an averaging of the electric field gradient, seen by the quadrupolar nucleus of interest. Therefore, *T. P. Das and E. L. Hahn* **[5]** considered this averaging by varying the z-component of the electric field gradient $eq = V_{zz}$ and the asymmetry parameter η of the stationary molecule (precisely its electric field gradient) with respect to the mean square of the torsional angle $\langle\theta^2(t)\rangle$, since $\langle\theta(t)\rangle = 0$ (1.8). Oscillations occur about the x- and y- principle axis of the stationary molecule, and are assumed to be small $\theta_x(t),\ \theta_y(t) \ll 1$.

$$\langle V_{zz}\rangle = V_{zz}\left[1 - \frac{3}{2}\left(\langle {\theta_x}^2(t)\rangle + \langle {\theta_y}^2(t)\rangle\right) - \frac{\eta}{2}\left(\langle {\theta_x}^2(t)\rangle - \langle {\theta_y}^2(t)\rangle + \frac{1}{2}(3-\eta)\langle {\theta_x}^2(t)\rangle\langle {\theta_y}^2(t)\rangle\right]\right.$$

(2.18)

$$\langle \eta\rangle = \frac{V_{zz}}{\langle V_{zz}\rangle}\left[\eta - \frac{3}{2}\left(\langle {\theta_x}^2(t)\rangle - \langle {\theta_y}^2(t)\rangle\right) - \frac{\eta}{2}\left(\langle {\theta_x}^2(t)\rangle + \langle {\theta_y}^2(t)\rangle + \frac{1}{2}(3-\eta)\langle {\theta_x}^2(t)\rangle\langle {\theta_y}^2(t)\rangle\right]\right.$$

The magnitude of $\langle\eta\rangle$ was always used to avoid negative values of $\langle\eta\rangle$.

If above equations (2.18) are inserted into the PAS formulation of the nuclear quadrupole interaction Hamiltonian (1.4) the following averaged Hamiltonian $\langle H_Q\rangle$ results:

$$\langle H_Q\rangle = \frac{eQ\langle V_{zz}\rangle}{4I(2I-1)}\left[3\mathrm{I}_z^2 - \mathrm{I}^2 + \langle\eta\rangle\left(\mathrm{I}_x^2 - \mathrm{I}_y^2\right)\right], \qquad (2.19)$$

where $eQ\langle V_{zz}\rangle$ is the averaged nuclear quadrupole coupling constant, containing the averaged z-component of the electric field gradient $\langle V_{zz}\rangle$ and $\langle\eta\rangle$ denotes the averaged asymmetry parameter.
The relation of $\langle {\theta_x}^2(t)\rangle$ resp. $\langle {\theta_y}^2(t)\rangle$ to temperature is done by means of the quantum mechanical harmonic oscillator already mentioned. This step is shown in section 2.3.2.3.

2.3.2.2 Numerical averaging of Hamiltonian

With the help of a numerical averaging implementation it is possible to consider oscillations around any predefined axis (Hamiltonian in the LABS). In addition, assumptions about small angles θ(t) ≪ 1, as in 2.3.2.1, are no longer necessary.

Thus equation 1.7, describing harmonic torsional oscillations was applied as follows:

Assumption of harmonic oscillation:

$$\theta(t) = \hat{\theta}(t)\sin(2\pi f_t t) = \hat{\theta}(t)\sin(2\pi t), \qquad (2.20)$$

where time t is a vector of dimension 1 X N ranging from 0 to 1 s, N is the number of sampling points. Only one period of the oscillation is considered, thus the torsional frequency f_t can be set to 1.

Averaging of Hamiltonian:

Calculation of the Hamiltonian for each sampling point N using the previous mentioned Bayer Hamiltonian (2.14 or 2.15) or the general LABS – formulation (2.17), and subsequent averaging (arithmetic mean).

Repeat previous steps for each peak amplitude $\hat{\theta}(t)$ of the torsional angle.

The numerical error of this implementation obviously depends on the number of sampling points N. The temperature-dependent peak amplitudes of the torsional angle $\hat{\theta}(t)$ must be related to temperature with the help of the quantum mechanical harmonic oscillator already mentioned. This step is introduced in section 2.3.2.3.

All previously introduced numerical implementations of the quadrupole interaction Hamiltonians as well as their averaging due to torsional oscillations will be evaluated and discussed in the results section.

2.3.2.3 Torsional's angle peak amplitude as a function of temperature

As already discussed in the introduction, the relationship between torsional oscillations and sample temperature can be described with the help of the quantum mechanical harmonic oscillator (equation 1.10) **[10]**:

$$hf_t\left(\frac{1}{2}+\frac{1}{e^{\frac{hf_t}{kT}}-1}\right) = 4\pi^2 {f_t}^2 A\langle\theta^2(t)\rangle \qquad (1.10)$$

Rearrangement of above formula gives:

$$\langle\theta^2(t)\rangle = hf_t\left(\frac{1}{2}+\frac{1}{e^{\frac{hf_t}{kT}}-1}\right)\frac{1}{4\pi^2 {f_t}^2 A} \qquad (2.21)$$

Furthermore, using relation $\langle\theta^2(t)\rangle = \frac{\hat{\theta}^2(t)}{2}$,

$$\hat{\theta}(t) = \sqrt{2hf_t\left(\frac{1}{2}+\frac{1}{e^{\frac{hf_t}{kT}}-1}\right)\frac{1}{4\pi^2 {f_t}^2 A}} \qquad (2.22)$$

Whereby, $f_t = f_{t,0}(1 - g\Delta t)$ in case of our investigated molecular crystals!

If the molecule-specific parameters: g, $f_{t,0}$, and *A* are known, it is possible to express the temperature dependence of the peak amplitude $\hat{\theta}(t)$ resp. the mean square $\langle\theta^2(t)\rangle$ of the time-dependent torsional angle $\theta(t)$ with the equations (2.21 and 2.22) described above.

2.3.3 Calculation of Qcc and η from NQR transition frequencies

In order to determine the parameters Qcc and η by means of "pure" nuclear quadrupole resonance spectroscopy, it is necessary to know at least two NQR transition frequencies **[41]**. The calculation of the nuclear quadrupole coupling constant Qcc and the asymmetry parameter η from measured NQR transition frequencies, precisely Transition 3 and 4, is now briefly explained.

Calculation of η:

The asymmetry parameter η can be easily calculated by forming the ratio Transition 4 / Transition 3. Once the ratio is formed, it can be assigned to a value of the asymmetry parameter. This assignment was done with the help of a lookup table and piecewise linear interpolation. To generate the lookup table the NQR transition frequency ratio, for different values of η (ranging from 0 to 1 with 1e6 sampling points) had to be calculated before.

Calculation of Qcc:

The calculation of Qcc is done with the previously calculated η and Transition 4. Therefore, the nuclear quadrupole interaction Hamiltonian (in PAS) must be rearranged without its nuclear quadrupole coupling constant being included (Qcc set to 1). After determining its eigenvalues and relation to Transition 4, the unknown nuclear quadrupole coupling constant Qcc can be obtained.

2.3.4 Numerical fitting approach

The fitting models described in section 2.2 assume that the asymmetry parameter of the observed molecule equals zero ($\eta = 0$). In fact, it remains equal to zero over the entire temperature range. In order to reject this assumption, a numerical fitting approach was implemented, considering ($\eta \neq 0$) and its temperature-dependent change.
The NQR transition frequency of interest (Transition 3 and Transition 4) is calculated with the help of the numerical averaging function introduced above (see 2.3.2.2), using the LABS-formulation of the Hamiltonian (see 2.3.1.3 equation 2.17).

Thus, the objective function to be minimized is given by:

$$\min_{param} \left\| v_{avg}(param, g, T)\big|_{T3,T4} - v_{meas}|_{T3,T4} \right\|_2^2 \qquad (2.23)$$

where, $v_{avg}(param, g, T)\big|_{T3,T4}$ are the calculated NQR transition frequencies (concatenated vector of Transition 3 and Transition 4) with minimization parameters: param = [$f_{t,0}$, A, Qcc, η] and the temperature coefficient g determined by Brown´s method (see section 2.2); $v_{meas}|_{T3,T4}$ contains the measured NQR transition frequencies of interest.

The objective function presented above considers both measured NQR transition frequencies, which is crucial since the nuclear quadrupole coupling constant as well as the asymmetry parameter have to be determined.

The above introduced objective function (2.23) was minimized using the nonlinear least-squares MATLAB solver **lsqnonlin** (trust-region-reflective algorithm). As termination tolerance **'TolFun'** was set to 1e-10, with an additional restriction of 80 iterations.

The following initial parameters and boundary conditions were applied:

Table 2.5: Initial parameters and boundary conditions of numerical fitting approach

	$f_{t,0}\ in\ THz$	$A\ in\ 10^{-44}\ in\ kgm^2$	$Qcc\ in\ MHz$	$\eta\ (1)$
BIPH3				
Initial parameters	1.5	0.05	684.6	0.09
Lower bounds	0	0	668.9	0.08
Upper bounds	10	10	700	0.5
BIPH3_OME				
Initial parameters	1.5	0.05	715	0
Lower bounds	0	0	700	0
Upper bounds	10	10	800	0.5

The boundary conditions and initial parameters of the quadrupole coupling constant and the asymmetry parameter were chosen based on the values already known, as listed in Table 2.2, whereby the initial parameters of $f_{t,0}$ and A were chosen on the basis of the fittings (Table 3.2) already made.

The parameters obtained in these fittings and their goodness of fit are presented in detail in the results section (Table 3.5).

2.4 Identifier scheme of different implementations

To keep the overview the following identifiers are used for different numerical and analytical implementations (Table 2.6), which were introduced in previous sections (section 2.2 and 2.3).

Table 2.6: Identifier scheme of used implementations

Identifier	Hamiltonian formulation/Fitting equation*	Averaging method	Assumptions	Color in plots
NABayer	Bayer (equation 2.14)	numerical (section 2.3.2.2)	$\eta = 0$, not constant	green
NABayerA	Bayer approx. (equation 2.15)	numerical (section 2.3.2.2)	$\eta = 0$, not constant small angle approximation	black
NALABS	LABS (equation 2.17)	numerical (section 2.3.2.2)	-	red
AAPASA	PAS (equation 1.4)	analytical (section 2.3.2.1)	small angle approximation	magenta
Bayer-Brown	Analytical Bayer-Brown-Model* (equation 2.8)	-	$\eta = 0 = constant$ small angle approximation	blue
Kushida-Brown	Analytical Kushida-Brown-Model* (equation 2.7)	-	$\eta = 0 = constant$ small angle approximation	green/arbitrary

Above introduced identifiers are applied to further analyses, especially in section 3.2.

3 Results

This chapter shows the most important findings of the above introduced methods applied to the measurement data. First, fitting parameters were determined using the analytical Kushida-Brown and Bayer-Brown models (equation 2.7 and 2.8). With the help of these fitting parameters the before-mentioned numerical implementations could be tested and compared. The influence of simplifications on the calculated, more precisely modelled NQR transition frequencies is shown. Finally, the numerical fitting approach (equation 2.23) was applied to measurement data, obtaining the fitting parameters A, $f_{t,0}$, Qcc and η. The practical benefits of numerical methods, more precisely the introduced numerical fitting approach, are also demonstrated. Furthermore, interesting facts regarding the underlying temperature-dependent torsional oscillations of the investigated molecules are shown.

3.1 Fitting Models

Figure 3.1 to Figure 3.4 show the fitting results of the Kushida-Brown resp. Bayer-Brown model (equation 2.7 & 2.8 applied to BIPH3 and BIPH3_OME Transition 3 and 4). The obtained fitting parameters (A, $f_{t,0}$ and v_Q) and goodness of fit are illustrated in Table 3.2.

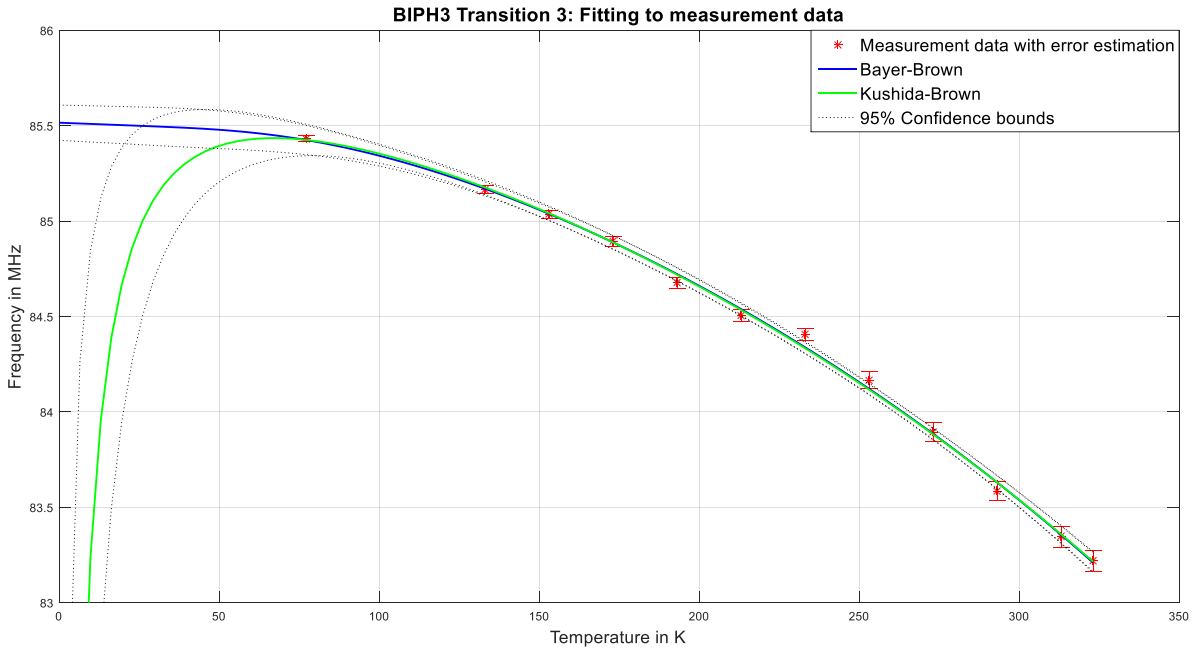

Figure 3.1: Fitting to measurement data (BIPH3 Transition 3; error estimation of measurement data included) with Bayer-Brown- resp. Kushida-Brown-Model

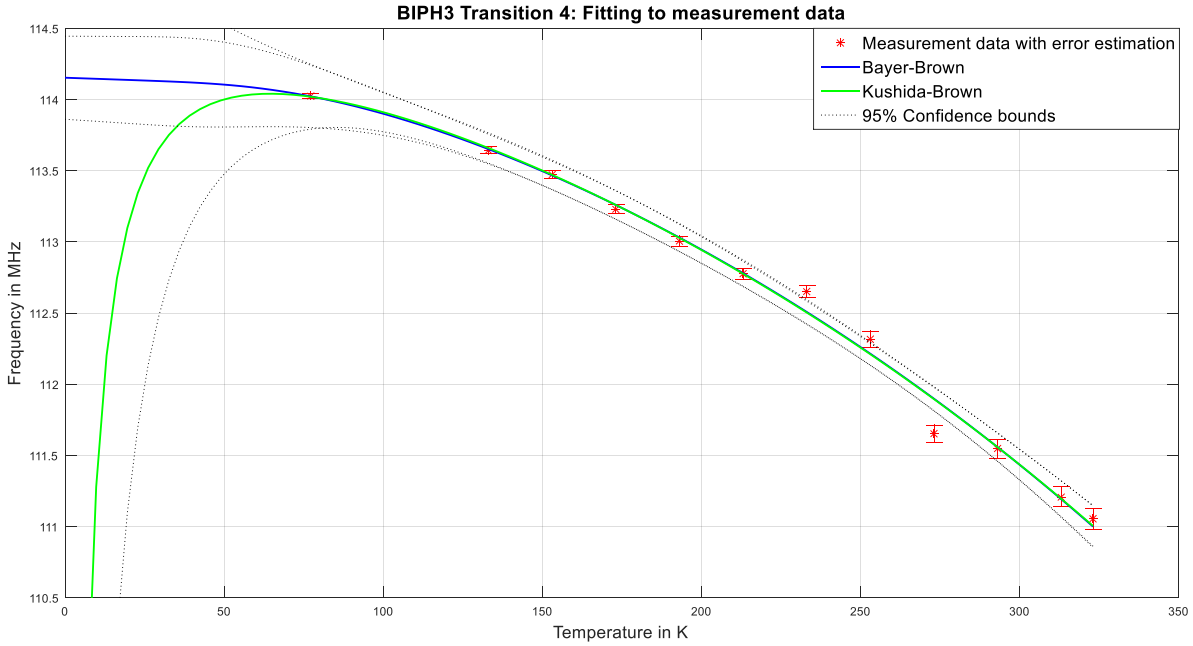

Figure 3.2: Fitting to measurement data (BIPH3 Transition 4; error estimation of measurement data included) with Bayer-Brown- resp. Kushida-Brown-Model

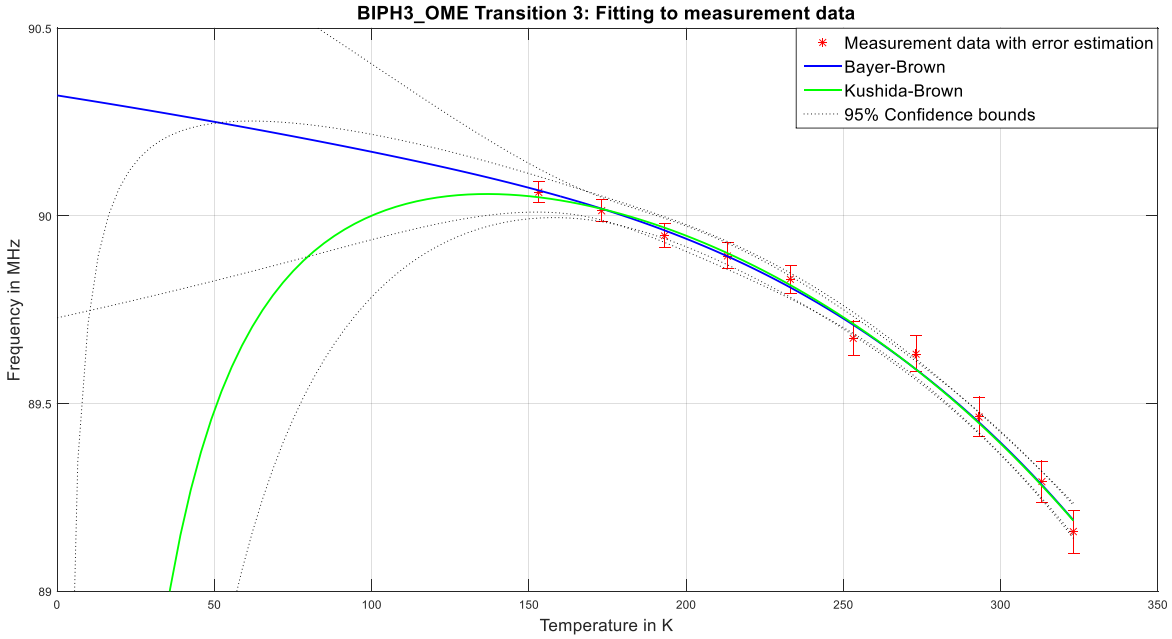

Figure 3.3: Fitting to measurement data (BIPH3_OME Transition 3; error estimation of measurement data included) with Bayer-Brown- resp. Kushida-Brown-Model

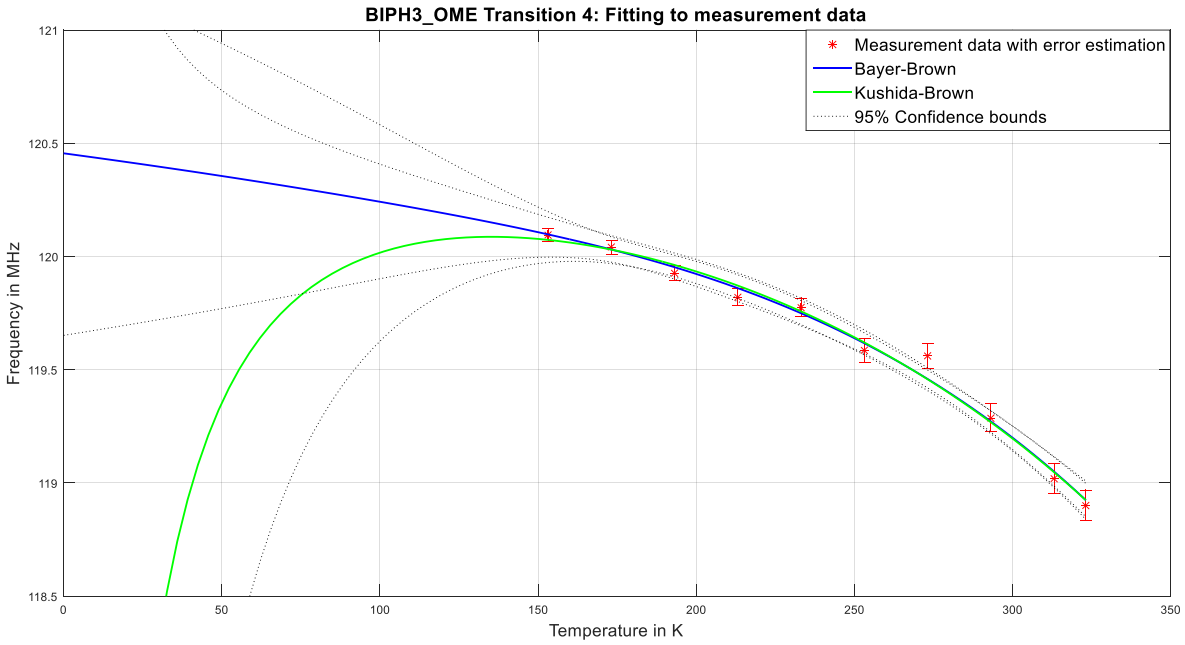

Figure 3.4: Fitting to measurement data (BIPH3_OME Transition 4; error estimation of measurement data included) with Bayer-Brown- resp. Kushida-Brown-Model

The temperature coefficients g of the torsional frequencies could be successfully determined with the help of Browns method and are listed in Table 3.1.

Table 3.1: Calculated temperature coefficients g with Brown´s-Method at evaluation point T_0

Sample	Transition	$g = \langle g \rangle \; in \; 1/K$	$T_0 \; in \; K$
BIPH3	3	**$9.46*10^{-4}$**	293.15
	4	**$8.87*10^{-4}$**	293.15
BIPH3_OME	3	**$18.12*10^{-4}$**	293.15
	4	**$18.03*10^{-4}$**	293.15

Table 3.2: Fitting parameters and goodness of fit obtained with Bayer-Brown´s- resp. Kushida-Brown´s model

Fitting Model	$A\ in\ 10^{-44}\ kgm^2$ *95% ci.*	$f_{t,0}\ in\ THz$ *95% ci.*	$v_Q\ in\ MHz$ *95% ci.*	$v(0\ K)\ in\ MHz$	$RMSE$	R^2_{Adj}
BIPH3						
Transition 3						
Bayer-Brown	**0.019** (0.003-0.035)	**5.168** (3.197-7.140)	**86.374** (86.056-86.692)	85.516	0.037	0.998
Kushida-Brown	**0.030** (0.012-0.048)	**4.194** (3.040-5.348)	**86.264** (86.069-86.458)	-Inf	0.038	0.997
Transition 4						
Bayer-Brown	**0.022** (-0.018-0.062)	**4.806** (0.754-8.859)	**115.250** (114.399-16.100)	114.153	0.104	0.989
Kushida-Brown	**0.031** (-0.010-0.072)	**4.048** (1.594-6.502)	**115.142** (114.596-15.687)	-Inf	0.104	0.989
BIPH3_OME						
Transition 3						
Bayer-Brown	**0.004** (-0.014-0.023)	**15.842** (-15.050-46.733)	**91.440** (88.155-94.725)	90.321	0.027	0.993
Kushida-Brown	**0.014** (0.002-0.027)	**9.046** (5.767-12.324)	**90.870** (90.470-91.271)	-Inf	0.028	0.992
Transition 4						
Bayer-Brown	**0.004** (-0.011-0.019)	**16.710** (-13.555-46.976)	**122.055** (117.753-26.357)	120.456	0.048	0.987
Kushida-Brown	**0.015** (-0.003-0.033)	**8.917** (4.368-13.466)	**121.148** (120.425-21.871)	-Inf	0.051	0.985

3.2 Forward Simulation and Model Comparison

Previously introduced numerical implementations of the quadrupole interaction Hamiltonians (PAS-, LABS-, Bayer-formulation, equations 1.4, 2.17, 2.14 & 2.15) and their averaging due to torsional oscillations (analytical and numerical averaging, sections 2.3.2.1 & 2.3.2.2) were used for simulations with the help of the before obtained fitting parameters of the Bayer-Brown model (BIPH3, Transition 3 and 4, see Table 3.2). It has to be mentioned that the quadrupolar coupling constant Qcc and the asymmetry parameter η had to be calculated with the knowledge of the fitting parameter ν_Q (NQR transition frequency of the static lattice) of Transition 3 and 4, to get the so-called "reference value*" for the analytical and numerical averaging functions. The Forward Simulation of different numerical implementations as well as the simulation of the analytical Bayer-Brown model (equation 2.8, also with above fitting parameters) are displayed in Figure 3.5 and Figure 3.6. All numerical simulations were carried out with Euler angles set to: $\alpha = 0°$, $\beta = \theta(t)$, $\gamma = 90°$, (oscillations about the x-principal axis of the stationary molecule) and 1250 sampling points N of the numerical averaging function of section 2.3.2.2.

The background of these simulations with an equivalent set of parameters is to show their deviations and to demonstrate the influence of certain simplifications on the calculated NQR transition frequencies. All further implementations (numerical and analytical Forward Simulations) are named according to the scheme in section 2.4.
The following simulations (with different reference values) and calculations (implementation deviations) are explained and discussed in detail in the discussion part. The whole analysis was focused on BIPH3 as BIPH3_OME would provide similar results.
* denotes the "static lattice parameter" of the torsional averaging process.

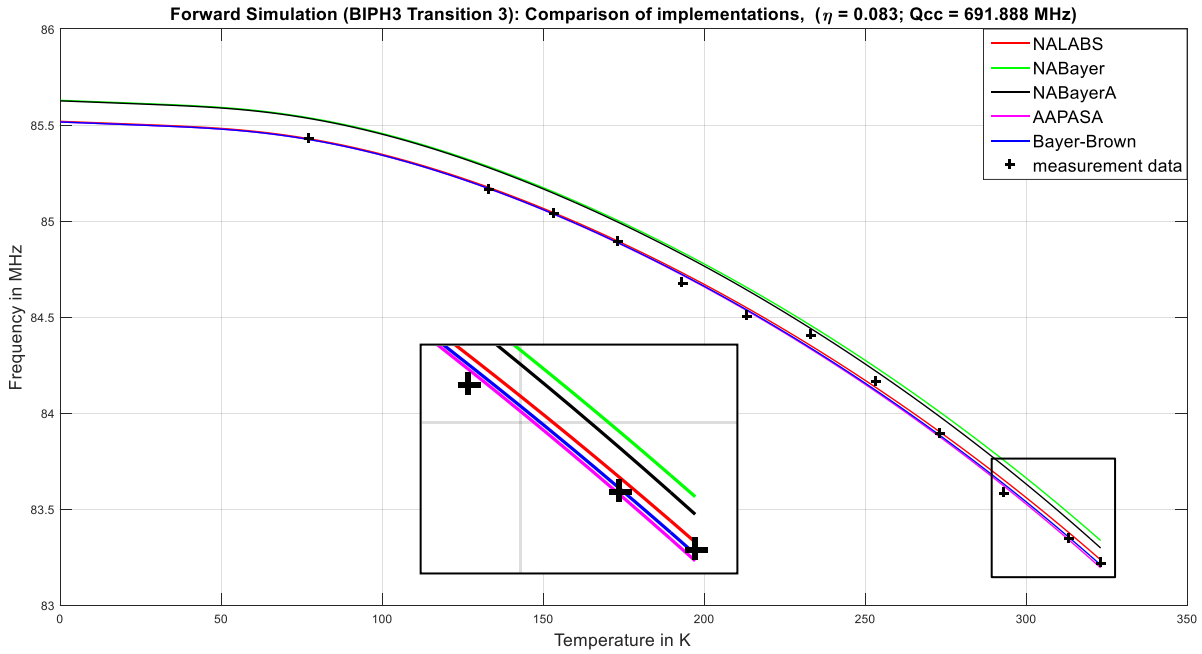

Figure 3.5: Forward simulation of different implementations with previously obtained fitting parameters (Bayer-Brown-Model, BIPH3 Transition 3) and reference values $\eta = 0.083$ resp. $Qcc = 691.888$ MHz.

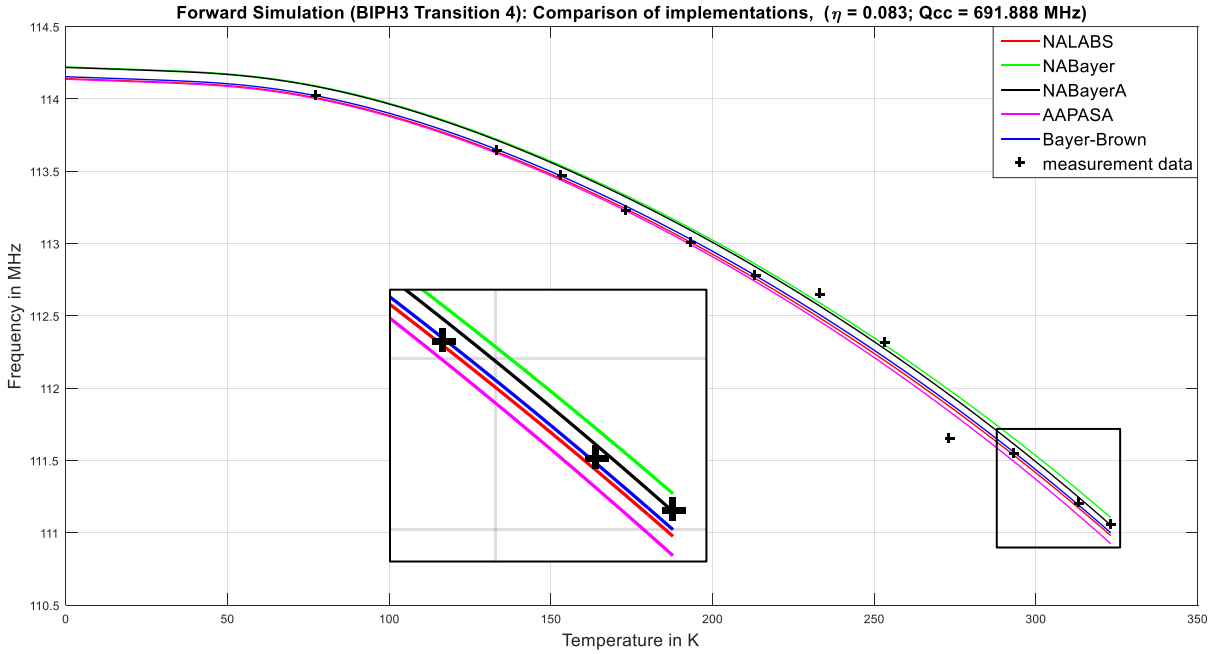

Figure 3.6: Forward simulation of different implementations with previously obtained fitting parameters (Bayer-Brown-Model, BIPH3 Transition 4) and reference values $\eta = 0.083$ resp. $Qcc = 691.888$ MHz.

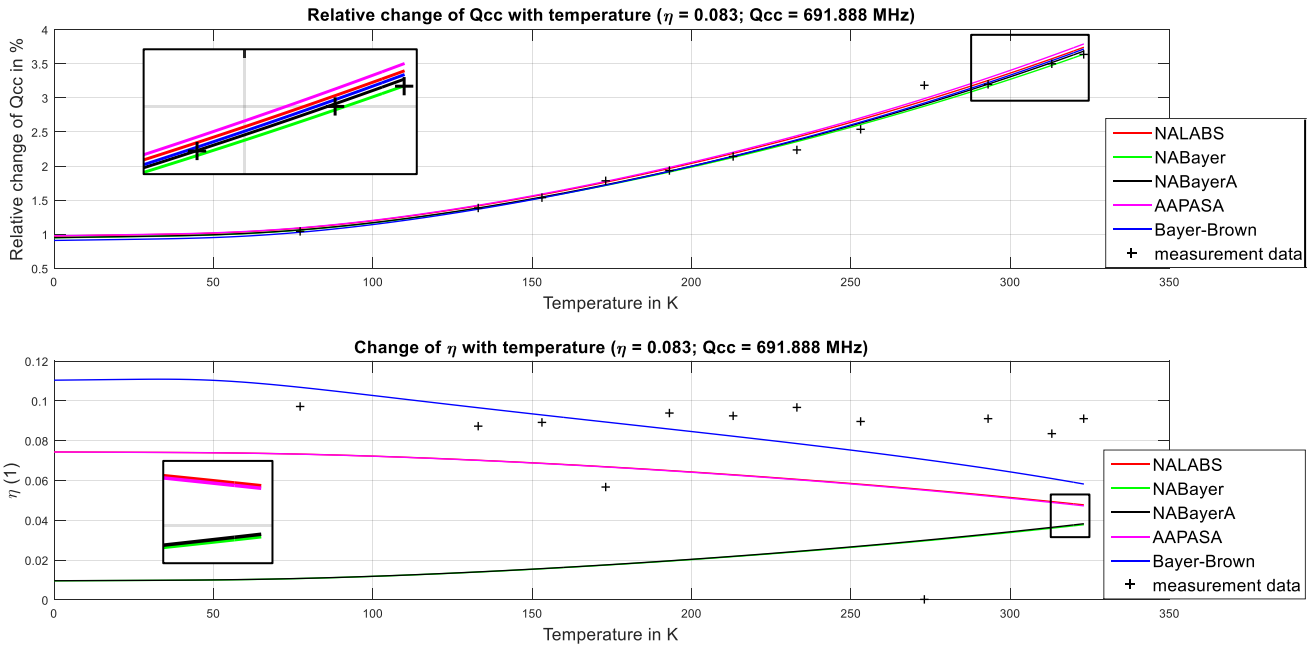

Figure 3.7: Change of Qcc and η of BIPH3 in terms of temperature (with $\eta = 0.083$, $Qcc = 691.888$ MHz as reference values).

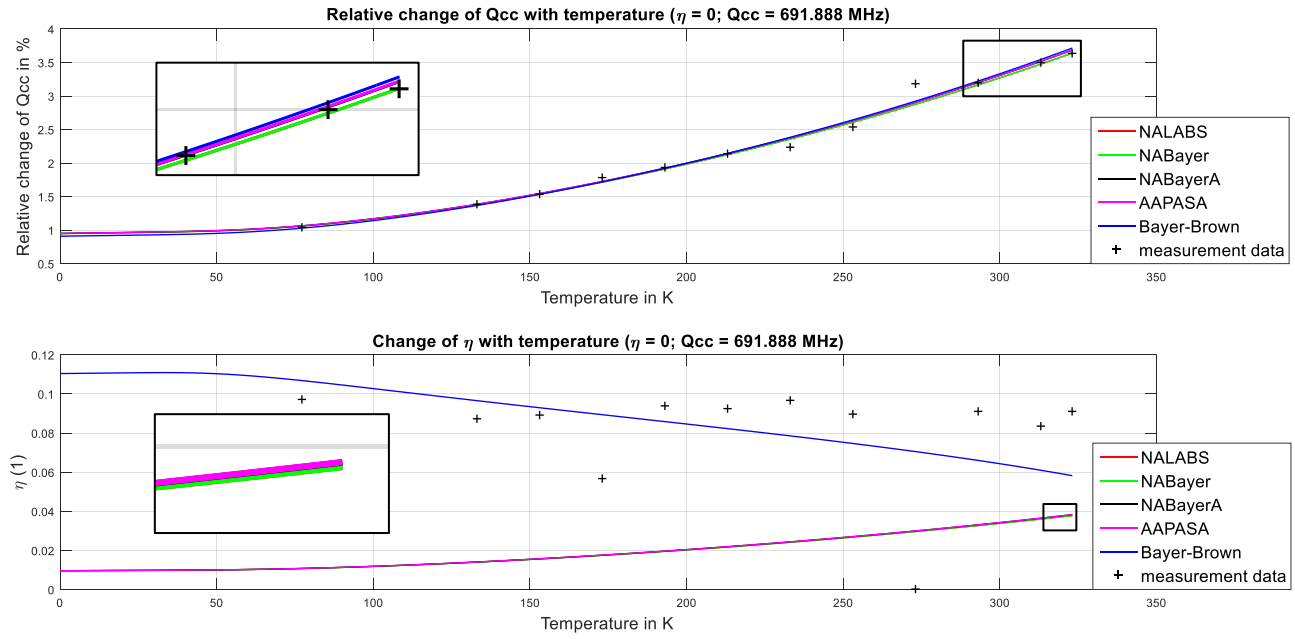

Figure 3.8: Change of Qcc and η of BIPH3 in terms of temperature (with $\eta = 0$, $Qcc = 691.888$ MHz as reference values)

Figure 3.7 & Figure 3.8 show the temperature dependence of Qcc and η for two different reference values ($\eta = 0.083$ and $\eta = 0$) for different implementations (see identifier table section 2.4). The relative change of Qcc can be defined as $(Qcc(static) - Qcc(T))/Qcc(static) * 100$.

The mean deviations (arithmetic mean) of Qcc and η between the NALABS and the NABayer implementation resp. the NABayerA and the AAPASA implementation are listed in Table 3.3 for both reference values mentioned above (Figure 3.7 & Figure 3.8).

Table 3.3: Mean Deviations of Qcc and η for different implementations

Qcc = 691.888 MHz, $\eta = 0.083$	**Mean Deviation of Qcc in kHz**	**Mean Deviation of η (1)**
NALABS vs. NABayer	$3.545*10^{2}$	$4.672*10^{-2}$
NABayerA vs. AAPASA	$3.677*10^{2}$	$4.642*10^{-2}$
Qcc = 691.888 MHz, $\eta = 0$	**Mean Deviation of Qcc in kHz**	**Mean Deviation of η (1)**
NALABS vs. NABayer	$1.007*10^{-9}$	$3.386*10^{-13}$
NABayerA vs. AAPASA	$1.029*10^{1}$	$1.55*10^{-5}$

The absolute differences between NABayer and NABayerA implementation (black dotted line) resp. AAPASA and Bayer-Brown (black solid line) are visualized in Figure 3.9 for both investigated Transitions (3, 4) of BIPH3. The calculated maximum deviations (T=323.15K) are 39kHz resp. 52kHz (black dotted line) and 15kHz resp. 76kHz (black solid line).

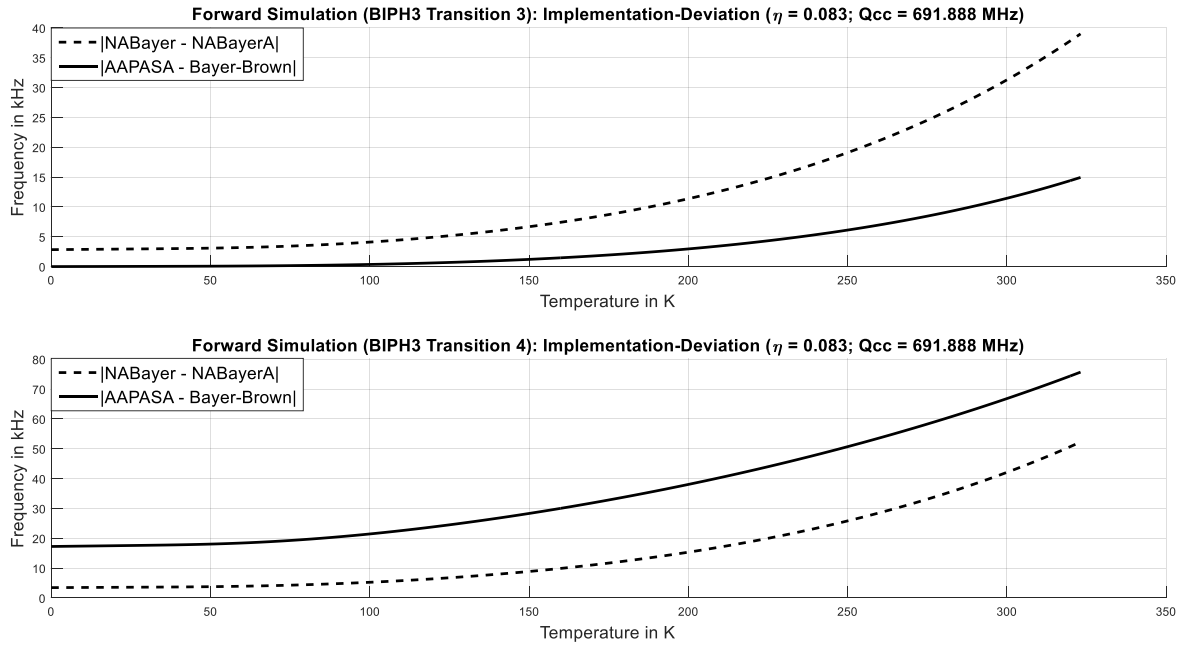

Figure 3.9: Implementation Deviations due to small angle approximation $\theta(t) \ll 1$ and constant η assumption in Bayer´s Model (with $\eta = 0.083$, $Qcc = 691.888$ MHz as reference values).

The implementation deviation caused by the finite number of sampling points N, used for the numerical calculation of the EFG´s averaging effect (section 2.3.2.2) are illustrated in Figure 3.10 and Table 3.4. Therefore, the absolute difference between the AAPASA and the NABayerA implementation (reference values $Qcc = 691.888$, $\eta = 0$) for different numbers of sampling points N (numerical averaging function section 2.3.2.2) ranging from 250 to 5000, were determined. Followed by a calculation of the maximum (Value at T=323.15 K) and mean (arithmetic mean) of above differences.

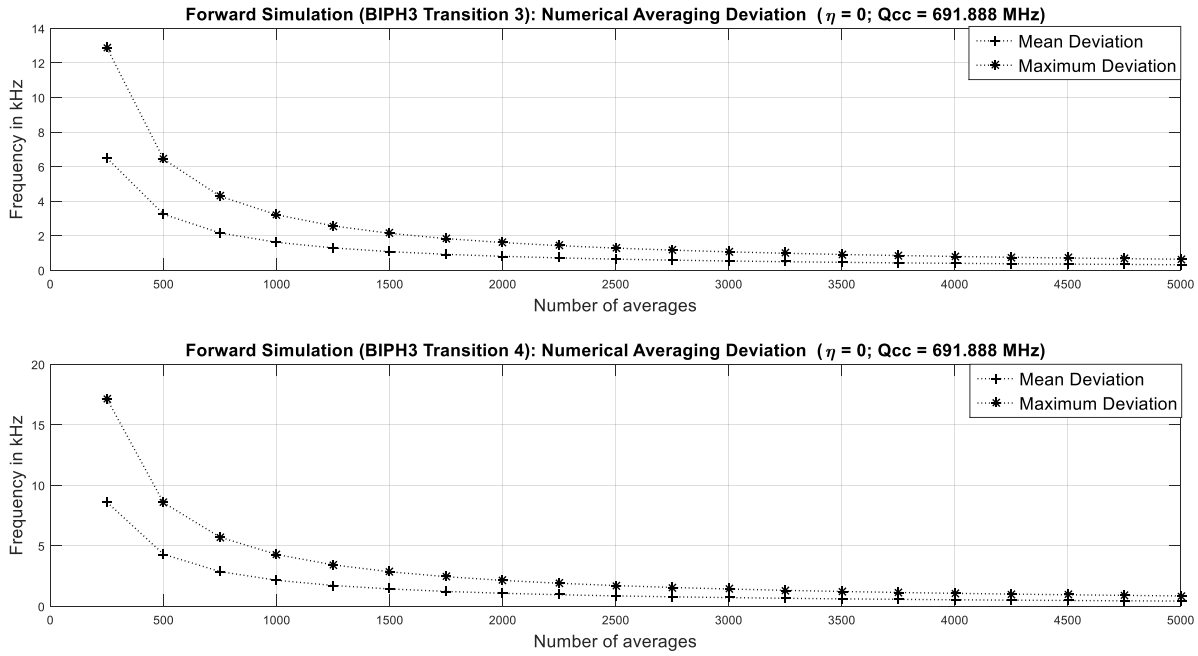

Figure 3.10: Implementation Deviations due to a finite number N of sampling points (numerical averaging function, with $\eta = 0$, $Qcc = 691.888$ MHz as reference values)

Table 3.4: Mean and Maximum Deviation due to numerical averaging function (section 2.3.2.2)

	Sampling points N	250	1250	5000
Transition 3	**Mean Deviation in kHz**	6.5	1.3	0.3
	Maximum Deviation in kHz	12.9	2.6	0.6
Transition 4	**Mean Deviation in kHz**	8.6	1.7	0.4
	Maximum Deviation in kHz	17.1	3.4	0.9

All before-mentioned Figures and Tables in this section are a summary of the analysis performed to work out the influence of different simplifications on simulated NQR transition frequency temperature dependency. A detailed explanation follows, as already mentioned, in the discussion part.

3.3 Numerical fitting approach

Figure 3.11 and Figure 3.12 show the fitting results of the numerical fitting approach of section 2.3.4 (BIPH3 and BIPH3_OME Transition 3 and 4). The obtained fitting parameters (A, $f_{t,0}$, Qcc and η) and goodness of fit are illustrated in Table 3.5. All numerical Forward Simulations, carried out in the course of the optimization process, were done with Euler angles set to: $\alpha = 0$, $\beta = \theta(t)$, $\gamma = 90$, (oscillations about the x-principal axis of the stationary molecule) and 1250 sampling points N of the numerical averaging function (recall section 2.3.2.2).

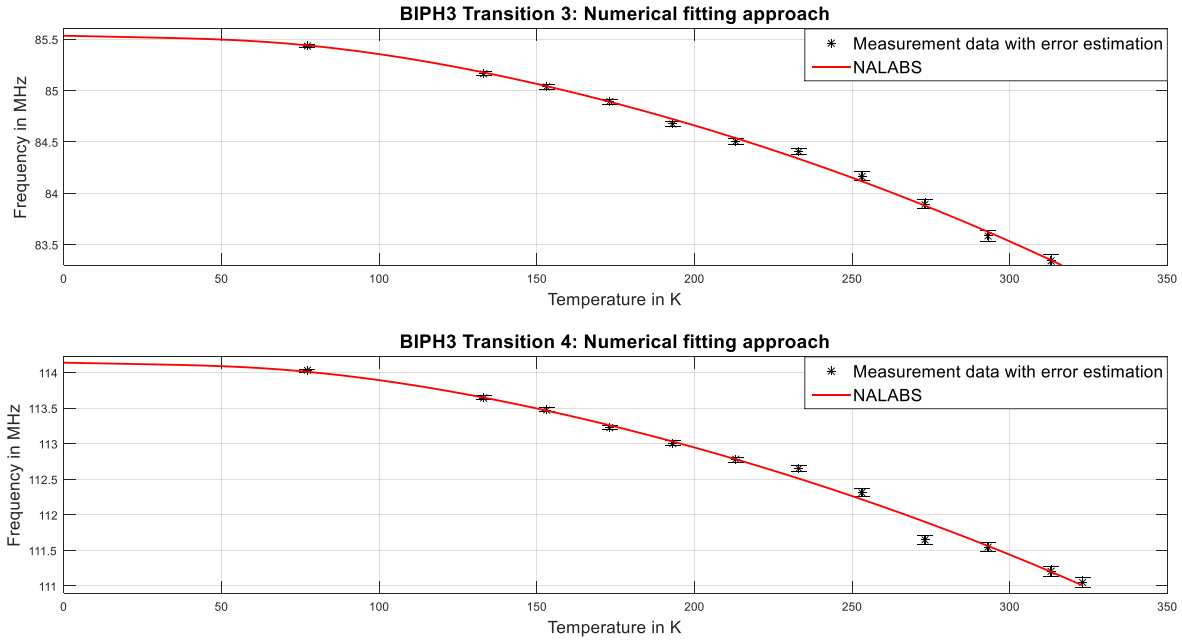

Figure 3.11: Fitting to measurement data (BIPH3 Transition 3 & 4; error estimation of measurement data included) with numerical fitting approach

To keep in mind, with this approach it is possible to fit Transition 3 and Transition 4 at once.

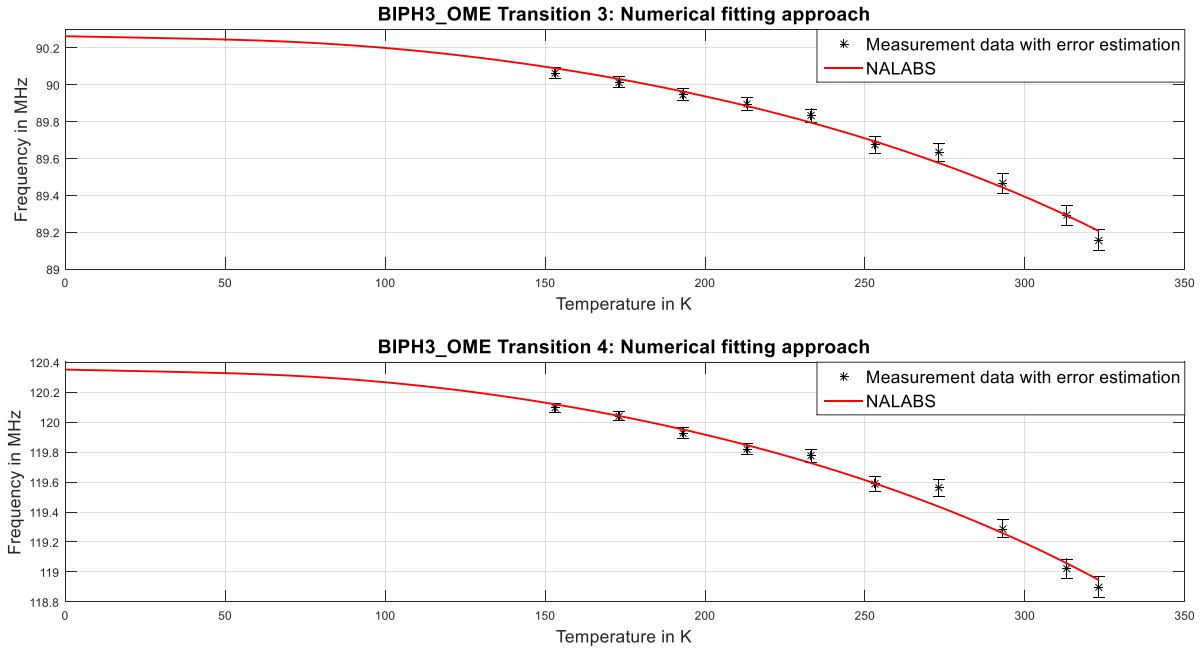

Figure 3.12: Fitting to measurement data (BIPH3_OME Transition 3 & 4; error estimation of measurement data included) with numerical fitting approach

Table 3.5: Fitting parameters and goodness of fit obtained with numerical fitting approach

Fitting Model	$A\ in\ 10^{-44}\ kgm^2$ *95% ci.*	$f_{t,0}\ in\ THz$ *95% ci.*	$Qcc\ in\ MHz$ *95% ci.*	$\eta\ (1)$ *95% ci.*	$RMSE$* Transition 3 Transition 4	$R^2{}_{Adj}$* Transition 3 Transition 4
BIPH3						
Transition 3 & Transition 4						
Numerical approach (NALABS)	**0.020** (0.001-0.039)	**5.007** (2.860-7.154)	**692.380** (689.430-695.331)	**0.104** (0.067-0.141)	0.040 0.110	0.997 0.988
BIPH3_OME						
Transition 3 & Transition 4						
Numerical approach (NALABS)	**0.056** (-0.182-0.294)	**4.894** (-5.056-14.844)	**724.283** (720.769-727.797)	**0.000** (-0.203-0.203)	0.039 0.063	0.984 0.977

*… $RMSE$ and $R^2{}_{Adj}$ were separately calculated for Transition 3 and Transition 4

3.4 Forward simulation of numerical models: Interesting Findings

The next subsection shows some interesting impacts on NQR transition frequency temperature-dependency, concerning different torsional oscillation directions. Furthermore, the temperature-dependent change of the torsional angle´s peak amplitude is displayed for both investigated molecules

3.4.1 LABS-Formulation and impact of asymmetry parameter η

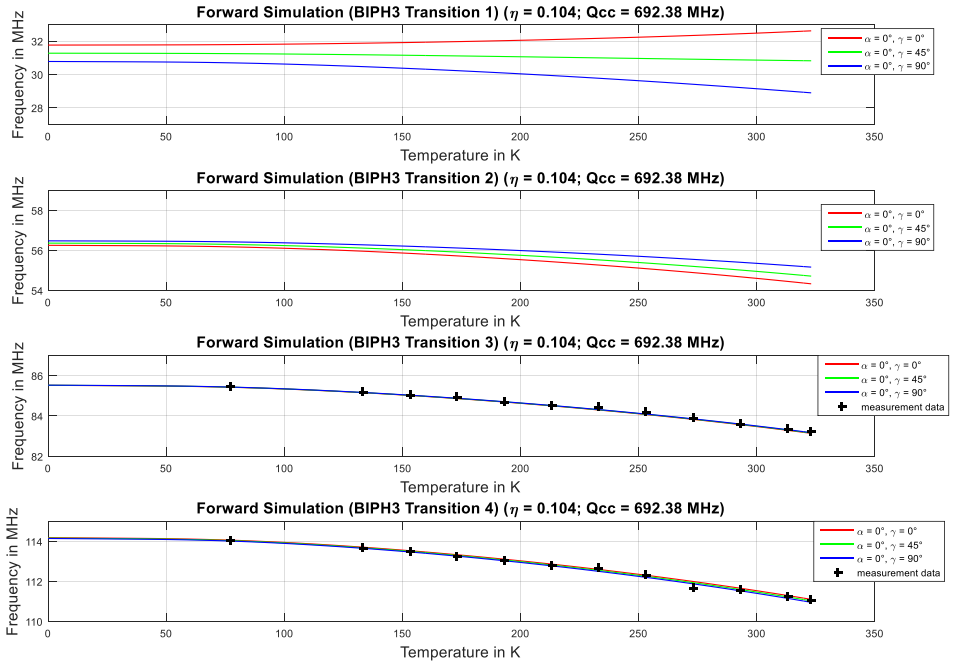

Figure 3.13: Influence of different torsional oscillation directions (α, $\beta = \theta(t)$, γ) on NQR transition frequencies (BIPH3 with $Qcc = 692.38$ MHz and $\eta = 0.104$ as reference values).

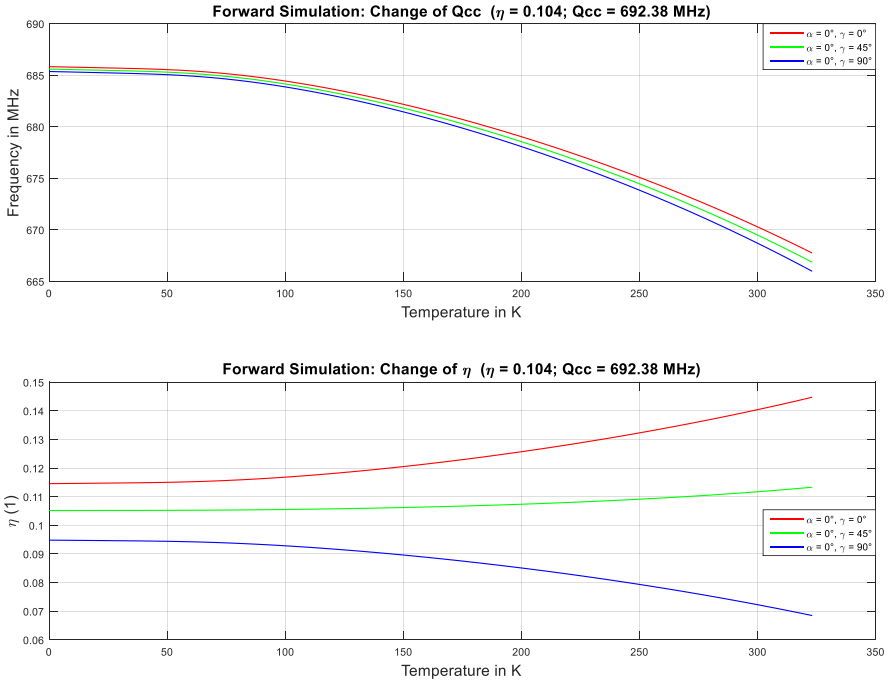

Figure 3.14: Influence of different torsional oscillation directions ($\alpha,\ \beta = \theta(t),\ \gamma$) on Qcc and η (BIPH3 with $Qcc = 692.38$ MHz and $\eta = 0.104$ as reference values).

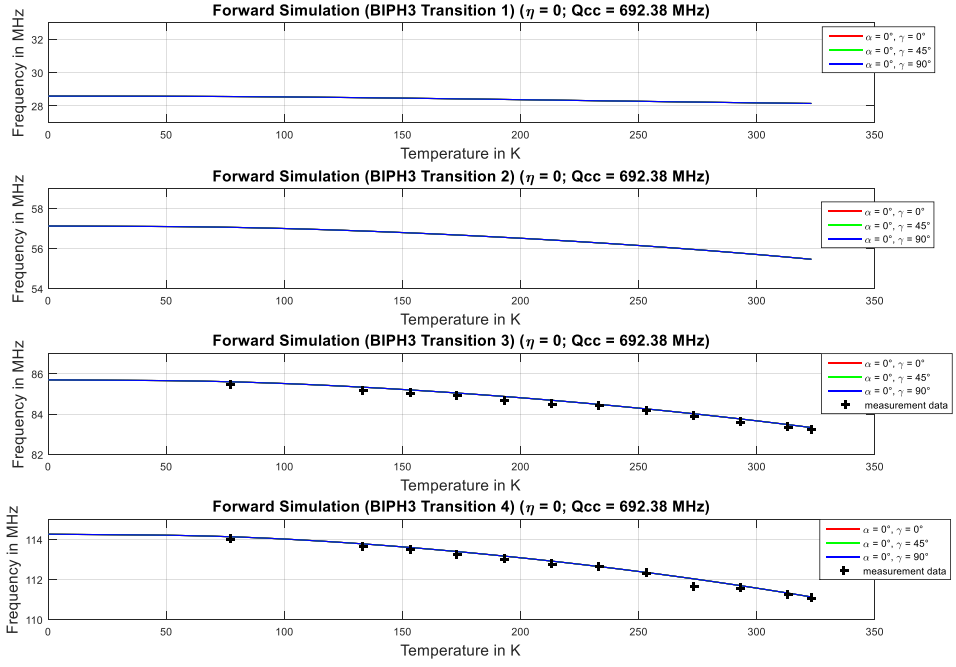

Figure 3.15: Influence of different torsional oscillation directions ($\alpha,\ \beta = \theta(t),\ \gamma$) on NQR transition frequencies (BIPH3 with $Qcc = 692.38$ MHz and $\eta = 0$ as reference values).

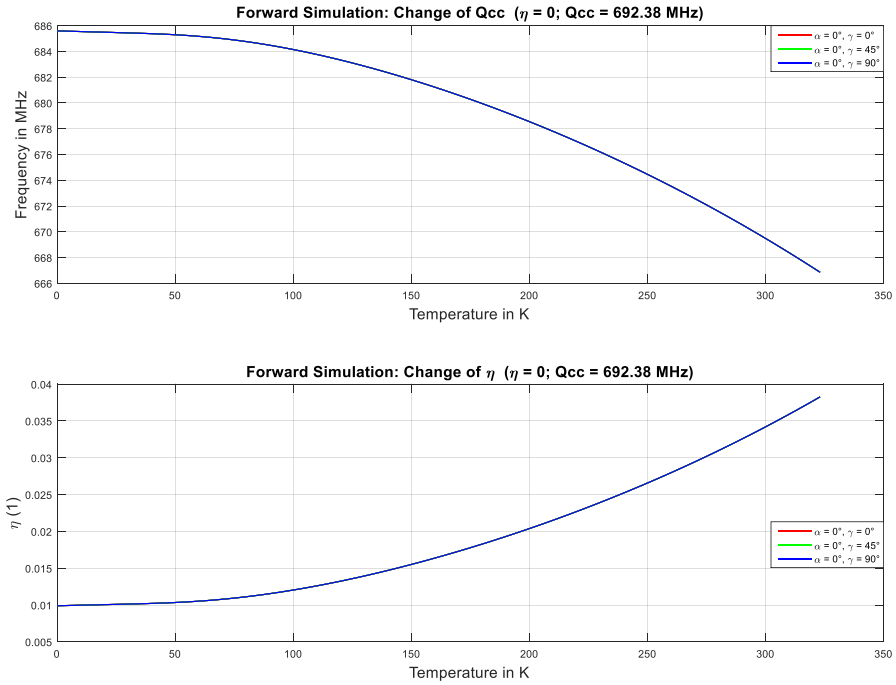

Figure 3.16: Influence of different torsional oscillation directions (α, $\beta = \theta(t)$, γ) on Qcc and η (BIPH3 with $Qcc = 692.38$ MHz and $\eta = 0$ as reference values).

The Forward Simulation of NQR transition frequencies were performed (Figure 3.13 and Figure 3.15) with the help of the Hamiltonian´s LABS-formulation (2.17) and the numerical averaging function (2.3.2.2), also called NALABS.

For this purpose, sampling points N of the numerical averaging function were set to 1250. All simulation parameters (A, $f_{t,0}$, Qcc and η) were those obtained from previous described numerical fitting approach of BIPH3 (Table 3.5 line 1). The influence of different torsional oscillation directions to Qcc and η are displayed in Figure 3.14 and Figure 3.16. However, Figure 3.15 and Figure 3.16 illustrate simulations assuming an axially symmetric electric field gradient ($\eta = 0$).

Qcc and η are the reference values (“static lattice parameter”) of the torsional averaging process.

3.4.2 Temperature-Dependency of torsional angle

The relationship between torsional oscillations and sample temperature can be described with the help of the quantum mechanical harmonic oscillator (recall equation 1.10 and section 2.3.2.3). This relationship, precisely the torsional angle´s peak amplitude $\hat{\theta}(t)$ in terms of temperature (equation 2.22), is therefore displayed in Figure 3.17 concerning both investigated molecular crystals.

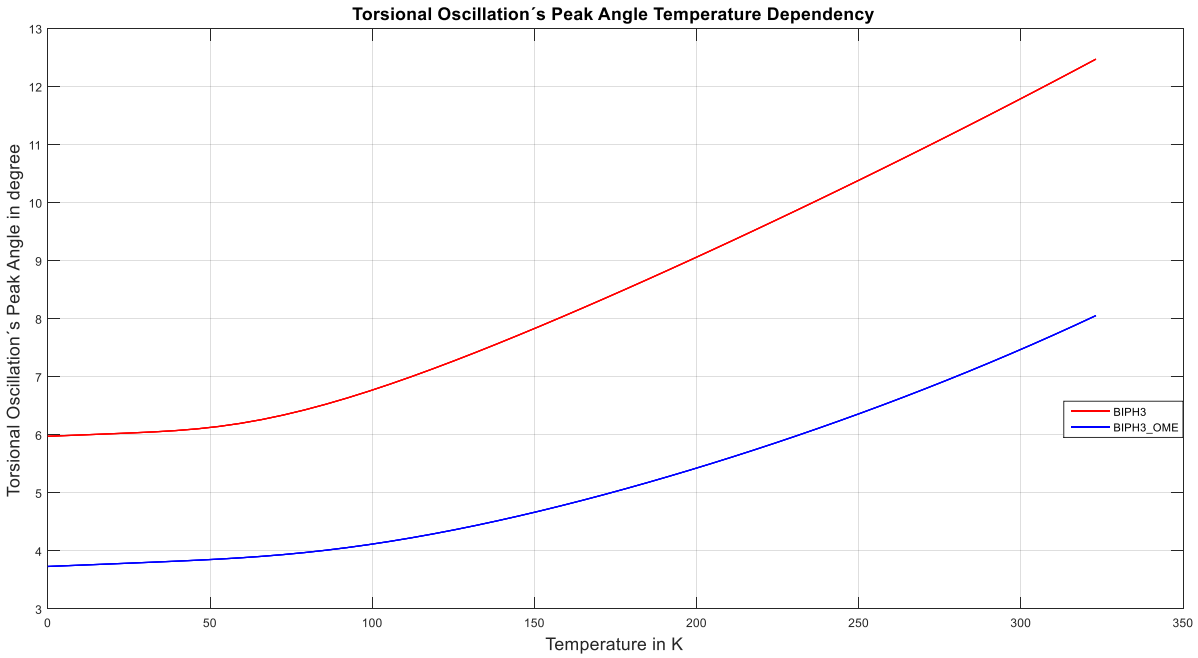

Figure 3.17: $\hat{\theta}(t)$ in terms of temperature for BIPH3 and BIPH3_OME

4 Discussion

Fitting Models

Figure 3.1 to Figure 3.4 visualize the fitting results of the analytical Bayer-Brown resp. Kushida-Brown model (BIPH3 and BIPH3_OME Transition 3 and 4). The trend of Kushida-Brown's model to minus infinity for low temperatures shows clearly why it's called the high temperature approximation. Both models seem to be valid describing the supposed decreasing NQR transition frequencies with increasing temperature (negative temperature coefficient) regarding their goodness of fit ($RMSE$, $R^2{}_{Adj}$ of Table 3.2) as well as their predictions being almost inside the estimated measurement errors (Table 2.3). In the case of BIPH3, the fitting parameters A, $f_{t,0}$ and v_Q of both models (Bayer-Brown and Kushida-Brown) are comparable in contrast to BIPH3_OME, where the estimated torsional frequency $f_{t,0}$ of Bayer-Brown's model is almost twice as large as that of Kushida-Brown's (see Table 3.2). One reason is surely the missing of measurement points of BIPH3_OME in the low-temperature range < 153.15 K, in contrast to BIPH3 having points at 133.15 K and 77.15 K too.

All fitting parameters of BIPH3 and previously calculated g-parameters (Table 3.1), having rationally orders of magnitude:

-g-values for molecular solids fall typically in the range of (0.0005 to 0.0015 K^{-1}) **[29**, **27]**: Thus, obtained values range from $\sim$ 0.0009 to 0.0018 K^{-1}

-The equivalent moment of inertia A is reported in magnitudes of order $10^{-45}\ \mathrm{kgm}^2$ for solid chlorine in *Nakamura and Chihara* **[42]** or dichloroethylene in *Bayer* **[10]**. Unfortunately, calculated values for BIPH3 or BIPH3_OME couldn't be found so far: The fitted A are in the order of $10^{-46}\ \mathrm{kgm}^2$, thus one order of magnitude below the values for solid chlorine or dichloroethylene.

-Usually normal modes with torsional frequencies below $150\ \mathrm{cm}^{-1} = 4.5\ 10^{12}\ \mathrm{Hz}$ contribute significantly to NQR transition frequency's temperature dependency **[27]**: So, the fitted torsional frequencies $f_{t,0}$ seem to be on the upper limit of supposed values.

The NQR transition frequency of the static lattice v_Q is always greater than that at 0 K (scale of 1 MHz), pointing out that the NQR transition frequency of the static lattice is not the same as the transition frequency at 0 K, a frequently used assumption in NQR transition frequency temperature dependence modeling processes!

Despite many simplifications of both models used, the fitted parameters seem to be plausible in their magnitudes. However, they should not be interpreted as valid physical parameters due to a variety of assumptions.

Model Comparison

To show the influence of frequently used simplifications on the modeled NQR transition frequencies temperature dependency, different implementations were compared (Figure 3.5 and Figure 3.6). Both Bayer implementations (NABayer and NABayerA) show a significant offset in both figures, which is due to the fact that they assume an axially symmetric electric field gradient of the static lattice (reference value). This fact is also illustrated in Figure 3.7 and Figure 3.8, where the change of η is the same for different reference values ($\eta = 0.086$ vs. $\eta = 0$). However, the numerical averaging function (section 2.3.2.2) as well as the analytical averaging (section 2.3.2.1) lead to a change of η with temperature, which is not the case for analytical models because of Bayer's assumptions (η equals zero over the entire temperature range: section 1.3).
At this point it is important to mention that due to the knowledge of two transitions it was possible to calculate the variation of Qcc and η in terms of temperature also for the Bayer-Brown model (analytical model equation 2.8), even though the model itself does not consider varying η (constant η assumption). Obviously, this issue results in an offset in calculated η of Bayer-Brown (blue solid line in Figure 3.7) compared to NALABS and AAPASA implementations. Qcc and η of the measurement data shows plausible order of magnitude, but they are strongly influenced by measurement errors (see section 2.1.2).
The analytical (AAPASA) and numerical averaging implementations (NALABS) have a similar trend compared with the simulated analytical Bayer-Brown model (Figure 3.5 Figure 3.6), but they don't yield the same results due to Bayer's assumptions. Values of the AAPASA and NALABS implementations differ exponentially with increasing temperature. This is due to the small angle approximation in the AAPASA and the implementation deviation caused by the numerical averaging function of the NALABS implementation.
Thus, to show the influence of different simplifications/assumptions on modeled NQR transition frequency as well as to check the plausibility of different numerical implementations, the following analyses were carried out:

1. The mean deviations of Qcc and η between the NALABS and NABayer resp. the NABayerA and the AAPASA implementation were calculated and listed in Table 3.3:

-In the case of $\eta = 0$ the NALABS and the NABayer coincide like expected, because the mean errors of Qcc and η are in the range of numerical errors (Table 3.3, line 3).
That's not the case for the Mean Deviations between the NABayerA and the AAPASA. In fact, the main difference between both implementations (for $\eta = 0$) is the used numerical averaging function (section 2.3.2.2).

2. Consequently, the absolute difference of these implementations could be used to calculate the deviation caused by a finite number of sampling points N of the numerical averaging function. The evolution of the mean and maximum values of the deviation is displayed in Figure 3.10 and listed in Table 3.4.

3. The impact of the small angle approximation as well as the constant η assumption of *Bayer* **[10]** could be investigated as follows:

   -The only difference between the NABayer and the NABayerA implementation is the assumption of small angles. Thus, calculating the absolute difference between both implementations (black dotted line) makes it possible to get information regarding the assumption´s impact. Figure 3.9 displays the calculated deviations.

   -Calculation of the absolute difference between the AAPASA implementation and the analytical Bayer-Brown model gives the deviation due to a constant eta assumption, because the analytical Bayer-Brown model doesn't account for that change. Both models assume small angles, so this calculation will be supposed to be valid showing the influence of the constant η assumption. The evolution of the deviation in terms of temperature is also shown in Figure 3.9 (black solid line).

Summarized, three simplifications were investigated: Namely, the influence of a finite number of sampling points N (numerical averaging function), the assumption of small angles and the impact of the constant η assumption (both cited in *Bayer* **[10]**) on modeled NQR transition frequencies temperature dependency. The implementation's maximum deviation due to a finite number of sampling points N could be kept below 3.5 kHz using N = 1250, which is smaller than the frequency resolution of the measurement data (10 kHz of BIPH3 and 50 kHz of BIPH3_OME). Therefore, every numerical simulation was at least carried out with 1250 sampling points! In comparison, the small angle approximation and constant η assumption lead to a

maximum deviation of max. 52 kHz resp. 76 kHz. So, they are in the order of magnitude of the measurement's data error estimation (Table 2.3). However, all deviations mentioned so far increase exponentially with temperature since they depend on the mean square resp. peak torsional angle of the EFG's oscillation.

Consequently, the introduced NALABS implementation can be seen as the best choice of above implementations regarding modeling the NQR transition frequency temperature dependence, since it gets rid of the small angle- and constant η assumption.

Numerical Fitting Approach

The Application of the novel numerical fitting approach to the measurement data is illustrated in Figure 3.11 resp. Figure 3.12 with its fitting parameters A, $f_{t,0}$, Qcc and η and goodness of fit listed in Table 3.5. The Parameters A, $f_{t,0}$ obtained are comparable to those of the analytical Bayer-Brown resp. Kushida-Brown model in case of BIPH3, whereas in case of BIPH3_OME the obtained parameters have slightly different values. Moreover, the obtained parameters of BIPH3_OME are comparable to those of BIPH3 which is plausible since BIPH3_OME is only a small modification of BIPH3.
The estimated quadrupole coupling constant as well as the asymmetry parameters have also reasonable values compared to values already known (Table 2.2).
As already mentioned, works this numerical fitting approach without an assumption of small angles resp. constant η (NALABS), resulting in the possibility of a more precise determination of fitting parameters under condition of a sufficient number of sampling points N. Another advantage is the consideration of both transitions, which makes it more robust against measurement errors (outliers, small amount of measurement points). However, longer processing times (~factor 100 compared to analytical evaluation) due to the evaluation of the numerical averaging function (solving eigenvalue problems) can be seen as a drawback.
Since there are many simplifications regarding the modeling process (one normal mode assumption, linearly varying torsional frequency, limitation to 80 iterations to shorten processing time) the obtained parameters shouldn't be interpreted as valid physical parameters.

Interesting Findings and benefits of numerical simulations

The influence of different torsional oscillation directions concerning the modelled NQR transition frequencies is visualized in Figure 3.13 and Figure 3.15. Therefore, the Euler angle γ got adapted to force the molecule to oscillate about the x-principle axis ($\gamma = 90°$), about the y-principle axis ($\gamma = 0°$) and finally about an axis which is lying between the x- and y- principle axis of the LABS ($\gamma = 45°$). The oscillation direction has an impact on the averaging effect of Qcc and η in case of axially asymmetry (Figure 3.14). Thus, η changed in opposite directions with increasing temperature, comparing oscillation directions of $\gamma = 0°$ and $\gamma = 90°$. This behavior had especially an impact on Transition 1 ($\gamma = 0°$), having a positive temperature coefficient. NQR transition frequencies with positive temperature coefficients were also reported in the literature *Nakamura et. al* **[19]** related to pi-bonding and hydrogen bonding. However, no literature could be found describing that special case caused due to torsional oscillations. Qcc and η in Figure 3.16 behave the same for different oscillation directions in case of axially symmetry, indicating that the deviation from axial symmetry caused the positive temperature coefficient of transition 1.
Before-mentioned observations are simulation results of arbitrary scenarios of molecular motions, which might not be observable in the investigated compounds.

The whole modelling process mentioned so far accounts for torsional oscillations of molecules about pre-defined axes. These oscillations are supposed to become greater with increasing temperature and are based on the mean energy of the quantum mechanical harmonic oscillator. Therefore, the torsional oscillation peak angle in terms of temperature is illustrated in Figure 3.17 for both investigated molecules. BIPH3 has clearly a greater response to temperature than BIPH_OME with a maximum peak angle of about 12°, thus having a greater temperature coefficient in general.

With the help of numerical implementations it is possible to simulate all 4 possible NQR transition frequencies for different scenarios by knowing only two transition frequencies needed for the numerical fitting approach to obtain the simulation parameters Qcc and η. A further advantage can be considered the elimination of secular equations and the removal of small angle- and constant η assumption.

Simplifications and improvements

In the course of the modelling process several assumptions were made:

-Assumption of one torsional normal mode
-Torsional frequency varies linearly with temperature
-The principal directions of the EFG tensor coincide with the principle directions of the moment of inertia tensor
-Stretching Vibrations were assumed to do not contribute significantly to the EFG's averaging.

Therefore, for future modelling it would be preferable to adapt/skip at least two of above assumptions:

1. Calculation of the moment inertia tensor of the molecule to skip one fitting parameter and account for deviations of the principle axis directions w.r.t. to the principle axis directions of the moment of inertia tensor.

2. Additionally, gaining deeper knowledge of lattice dynamics is a crucial step to adapt future modeling processes. To be more precise, the influence of such vibrations on the change of the EFG must be clarified and analysed in detail. The interested reader is referred to *McEnnan and Schempp* **[43]** where a zero-wavevector analysis is carried out to find the vibrational amplitudes of individual molecules regarding normal mode vibrations of the crystal.

Conclusion

In the course of this thesis it was possible to model the NQR transition frequency temperature dependence of BIPH3 and BIPH3_OME quantitatively with the help of analytical (Bayer-Brown and Kushida-Brown model) and numerical implementations (NALABS). The above introduced novel numerical fitting approach can be seen as a comprehensive tool for future investigations as arbitrary oscillation directions can be considered without making assumptions of small angles and constant η. Furthermore, different simulated torsional oscillation directions have an impact on the averaging effect of Qcc and η in case of axially asymmetry, resulting (e.g. for $\gamma = 0°$) in positive temperature coefficients for the lowest transition of BIPH3. Up to now it was not reported (considering the screened literature) that different torsional oscillation directions can lead to positive temperature coefficients of NQR transition frequencies.

5 Bibliography

[1] URL: http://www.conquer.at/about/project

[2] Christian Gösweiner et al**.,**Tuning Nuclear Quadrupole Resonance: A Novel Approach for the Design of Frequency-Selective MRI Contrast Agents, Physical Review X 8, 021076 (2018)

[3] *B. H. Suits*: Nuclear Quadrupole Resonance Spectroscopy.
Handbook of Applied Solid State Spectroscopy. Springer Verlag (2006)

[4] Paul Josef Krassnig: Charakterisierung von Antimonit als Referenzsystem für Nuclear Quadrupole Resonance Spectroscopy, Bachelor Thesis at Institute of Medical Engineering (2016)

[5] *T. P. Das, E. L. Hahn*: Nuclear quadrupole resonance spectroscopy, Solid state physics. Supplement 1, Academic Press Inc. (1958)

[6] Scharfetter H, Petrovic A, Eggenhofer H and Stollberger R 2014 A no-tune no-match wideband probe for nuclear quadrupole resonance spectroscopy in the VHF range Meas. Sci. Technol. 25 125501

[7] Hermann Scharfetter, An electronically tuned wideband probehead for NQR spectroscopy in the VHF rang, Journal of Magnetic Resonance, Volume 271, October 2016, p 90-98

[8] R. P. Feynman, R. B. Leighton, M. Sands: Quantenmechanik, Feynman-Vorlesungen über Physik, Band 3, Oldenbourg Verlag (2007)

[9] DEHMELT, H. G., u. H. Krüger: Naturwiss. 37, 111 (1950), Z. Physik
129**,** 401 (1951)

[10] H. Bayer, Zeitschrift für Physik, Bd. 130, S. 227 - 238 (1951)

[11] Dean and Pound, J. Chem. Phys. 20, 195 (1952)

[12] T.C. Wang, Pure Nuclear Quadrupole Spectra of Chlorine and Antimony Isotopes in Solids, Phys. Rev. 99, 566 (1955)

[13] R. F. Tipsword, E. L. Wilkinson, AND W. G. Moulton, Temperature Dependence of the Pure Quadrupole Frequency and Spin-Lattice Relaxation Time of p-Dibromobenzene, J. of Chem. Physics, Vol. 41. Nr. 9 (1964)

[14] R. W. Ward, C. D. Williams, and R. F. Tipsword, Asymmetry Parameters and the Temperature Dependence of the PQR Frequencies of I^{127} in SnI_4, J. of Chem. Physics, Vol. 51. Nr. 2 (1969)

[15] M. S. Vijaya and J. Ramakrishna, Motional Averaging of Electric Field Gradients. Temperature Dependence of NQR in Sodium Chlorate and Copper Chlorate, physica status solidi (b) 55(2):697 - 701 (February 1973)

[16] K. R. Sridharan et. al, ^{35}Cl NQR in $N_3P_3Cl_4Ph_2$ and $N_3P_3Cl_4(NMe_2)_2$, Polyhedron Vol. 3, No. 7, PP. 867-870, (1984)

[17] Mohammed Hossein Ala Amjadi, K. P. Ramesh, N. Rajendra Kumar and J. Ramakrishna*, Temperature dependence study of chlorine NQR frequency and spin–lattice relaxation time in 2-amino,-3,5-dichloropyridine, Magn. Reson. Chem. 37, 693–700 (1999)

[18] Ramesh KP, Suresh KS, Raghavendra Rao C, Ramakrishna J. Pressure and temperature dependence of the chlorine NQR in caesium and sodium chlorates. Magn Reson Chem. 2008;46:525-533.

[19] D. Nakamura, R. Ikeda and M. Kubo, Anomalous temperature variation of NQR frequencies and bonding in metal complexes, Coordination Chemistry Reviews, 17 (1975) 281-316

[20] H. Nakayama, N. Nakamura, and H. Chihara, Temperature Dependence of 63Cu and 14N Nuclear Quadrupole Resonance Frequencies in Potassium Dicyanocuprate(I), Inorg. Chem. 1981, 20,4393-4391

[21] Juan Murgich, On the temperature dependence of the 14N NQR in KTCNQ, The Journal of Chemical Physics 70, 5354 (1979)

[22] B, Amitha Bai, Nuclear quadrupole resonance studies on impurity and substitution effects in some chlorine compounds, Mangalore University, 31/12/1992

[23] Kushida T, Benedek GB, Bloembergen N. Phys. Rev. 1956; 104: 1364.

[24] I.O. HALFORD, J. chem. Physics 15, 645 (1947)

[25] I. Tatsuzaki and Y. Yokozawa, J. Phys. Soc. Japan, 1957, 12, 802.

[26] Kushida T. J. Sci. Hiroshima Univ. 1955; A19: 327.

[27] R. J. C. Brown, Temperature Dependence of Quadrupole Resonance Frequencies under Constant Pressure. The Journal of Chemical Physics 32, 116 (1960)

[28] Ichishima, J. Chem. Soc. Japan, Pure Chem. Sect. 71, 607 (1950).

[29] V. S. S. Sastry and J. Ramakrishna, Temperature dependence of chlorine nuclear quadrupole resonance and internal motions in o-chloro-, m-chloro-, 2-chloro-5-nitro- and 4-chloro-3-nitro-benzoic acids, J. Chem. Soc., Faraday Trans. 2, 1978, 74, 2014-2018

[30] K. Rukmani and J. Jesu Jamila Rani, Temperature Dependence of Internal Torsional Frequencies in 3,4-Dichloro Nitrobenzene and 4-Chloro 2 Nitrophenol Using NQR Data, ACTA PHYSICA POLONICA A, No. 6, Vol. 116 (2009)

[31] URL:
https://chem.libretexts.org/Bookshelves/Physical_and_Theoretical_Chemistry_Textbook_Maps/Supplemental_Modules_(Physical_and_Theoretical_Chemistry)/Spectroscopy/Vibrational_Spectroscopy/Vibrational_Modes/Normal_Modes

[32] Steven H. Simon, The Oxford Solid State Basics, Oxford University Press

[33] URL: https://www.sigmaaldrich.com/austria.html

[34] Scharfetter, Hermann; Bödenler Markus; Narnhofer Dominik, A cryostatic, fast scanning, wideband NQR spectrometer for the VHF range, Journal of Magnetic Resonance 286 (2018) 148–157

[35] Felix Theyer, Temperature dependency of NQR transition frequency measurements, Bachelor Thesis at Institute of Medical Engineering (2016)

[36] URL: http://easyspin.org/easyspin/documentation/spinoperators.html

[37] Wolfgang Nolting, Grundkurs Theoretische Physik 5/1, Quantenmechanik Grundlagen, 8. Auflage, Springer Spektrum

[38] URL: https://de.mathworks.com/help/matlab/ref/eig.html?s_tid=srchtitle

[39] C.P. Slichter, Principles of Magnetic Resonance, Springer Verlag, 1990

[40] Denimar Possa, Anderson C. Gaudio, Jair C.C.Freitas, Numerical simulation of NQR/NMR: Applications in quantum computing, Journal of Magnetic Resonance 209 (2011) 250-260

[41] Janez Seliger, University of Ljubljana and 'Josef Stefan' Institute, Ljubljana, Slovenia, Nuclear Quadrupole Resonance, Theory, 1999 Elsevier Ltd.

[42] Nobuo Nakamura and Hideaki Chihara, Nucear Quadrupole Resonance Study of Molecular Motion and Intermolecular Forces in Solid Chlorine, Journal of the Physical Society of Japan, Vol. 22, No. 1, January, 1967

[43] M.M. McEnnan and Ellory Schempp, Lattice Vibration Motional Averaging in Nuclear Quadrupole Resonance of Molecular Crystals. I. the Zero-Wavevector Case, Journal of Magnetic Resonance 11, 28-45 (1973)

List of Figures

List of Tables